Finite Element Modeling of Hip Resurfacing Cup Deformation

By

Nathanael Murray Kesler

A thesis submitted to
the Faculty of Graduate Studies
in partial fulfilment of
the requirements for the degree of
Master of Science

Department of Biosystems Engineering
Faculty of Engineering
University of Manitoba
Winnipeg, Manitoba

December 2009

Abstract

Hip resurfacing arthroplasty is touted as an attractive alternative to total hip arthroplasty for treatment of severe joint pain and limited mobility in young patients because it is bone conserving and allows for a greater range of motion. There is concern in the orthopaedic community, however, regarding surgically-induced deformation of hip resurfacing cups. Cup deformation could potentially compromise the tight clearance between the femoral head and cup, resulting in increased wear, acoustic emissions, and joint binding. This phenomenon has been investigated both experimentally and with finite element analysis (FEA). Finite element studies have contributed significantly to our understanding of cup deformation, such as the effect of different cup dimensions on deformation results, but unfortunately such studies were deficient in a number of ways. The first objective of this thesis was to create a three-dimensional finite element model of resurfacing cup deformation that addressed the limitations of previous models pertaining to pelvic geometry, meshing, material properties, and cup insertion, in order to more fully elucidate cup deformation. The second objective was to demonstrate that two-dimensional characterization of cup deformation at the cup rim is insufficient, by more fully characterizing cup deformation in three-dimensions. The geometry was obtained via laser scanning and digital processing of a hemi-pelvis replica, meshing was performed without the use of shell elements, linear elasticity with strain-hardening after the onset of yielding was assigned to the cup and bone, and the most appropriate method for simulation of cup

insertion was determined via two-dimensional axisymmetric analyses. Also, cup deformation was characterized in three-dimensions. The key findings of this thesis are that bone yield behaviour has important implications on press-fitting simulation, and the cup deforms irregularly and possibly plastically during press-fitting. A three-dimensional finite element model of resurfacing cup deformation that addressed the limitations of previous models was successfully created. Measurement of deformation at the rim of the resurfacing cup for characterization of cup deformation is insufficient; full characterization of cup deformation in three-dimensions is necessary. Future work should incorporate clinical testing to obtain model inputs such as impact and muscle forces, as well as model validation.

Acknowledgments

There are many people who were involved in making this thesis what it is. First of all, I must thank Dr. Jason Morrison, for he put forth much effort in providing guidance throughout this thesis. Drs. Zhang and Luo also provided valuable input. In addition to these persons, there are several people who went out of their way in helping me along through this thesis. First of all, I would like to thank the members of the Concordia Joint Replacement Group (CJRG), especially Drs. Colin Burnell and Thomas Turgeon, and Mr. Martin Petrak, for their support and guidance. I would like to thank Dr. Peng for kindly allowing me to use his laser scanner and software for creation of the 3D model geometry in this thesis. My friends deserve mention, as they were a source of encouragement and advice. I am very thankful for the support of my family also. I gratefully acknowledge the financial support of MAFRI, NSERC, CJRG, MITACS, and The Manitoba Government.

Contents

List of Tables

List of Figures

Chapter 1

Introduction

This thesis involves finite element modeling of hip resurfacing cup deformation to address limitations of previous studies. The motivation for performing this research was to provide the orthopaedic community with a better understanding of how a resurfacing cup may deform during surgery. This chapter begins with relevant background information on hip replacement surgery and an overview of finite element analysis. That section is followed by the statement of the problem and objectives sections, which also discuss motivations for this thesis work. The final section of this chapter presents an overview of the material found in the thesis.

1.1 Background

Hip replacement surgery, also known as hip arthroplasty, is a procedure that dramatically improves the quality of life of patients suffering with severe joint pain and limited mobility. The main cause of joint pain is osteoarthritis, a crippling disease that is characterized by loss of articular cartilage, change (i.e., remodelling) of the bone underneath the carti-

lage (subchondral bone), and formation of fibrous and cartilaginous bony growths called osteophytes (Buckwalter and Etienne 2006; CIHI 2009). Hip replacement surgery involves replacement of the diseased and/or damaged joint tissue with a prosthesis that effectively forms a new ball-and-socket joint. The two main types of hip prostheses are total hip and hip resurfacing prostheses. The conventional total hip prosthesis consists of a metallic femoral stem and attached head that is implanted into the femur (thigh bone), and a plastic-lined metallic acetabular shell that is implanted into the acetabulum of the pelvis, as shown in Figure 1. The metal-on-metal hip resurfacing prosthesis, illustrated in Figure 2, consists of a cobalt-chromium (CoCr) resurfacing head that caps the head of the femur, and a CoCr cup that is implanted into the acetabulum.

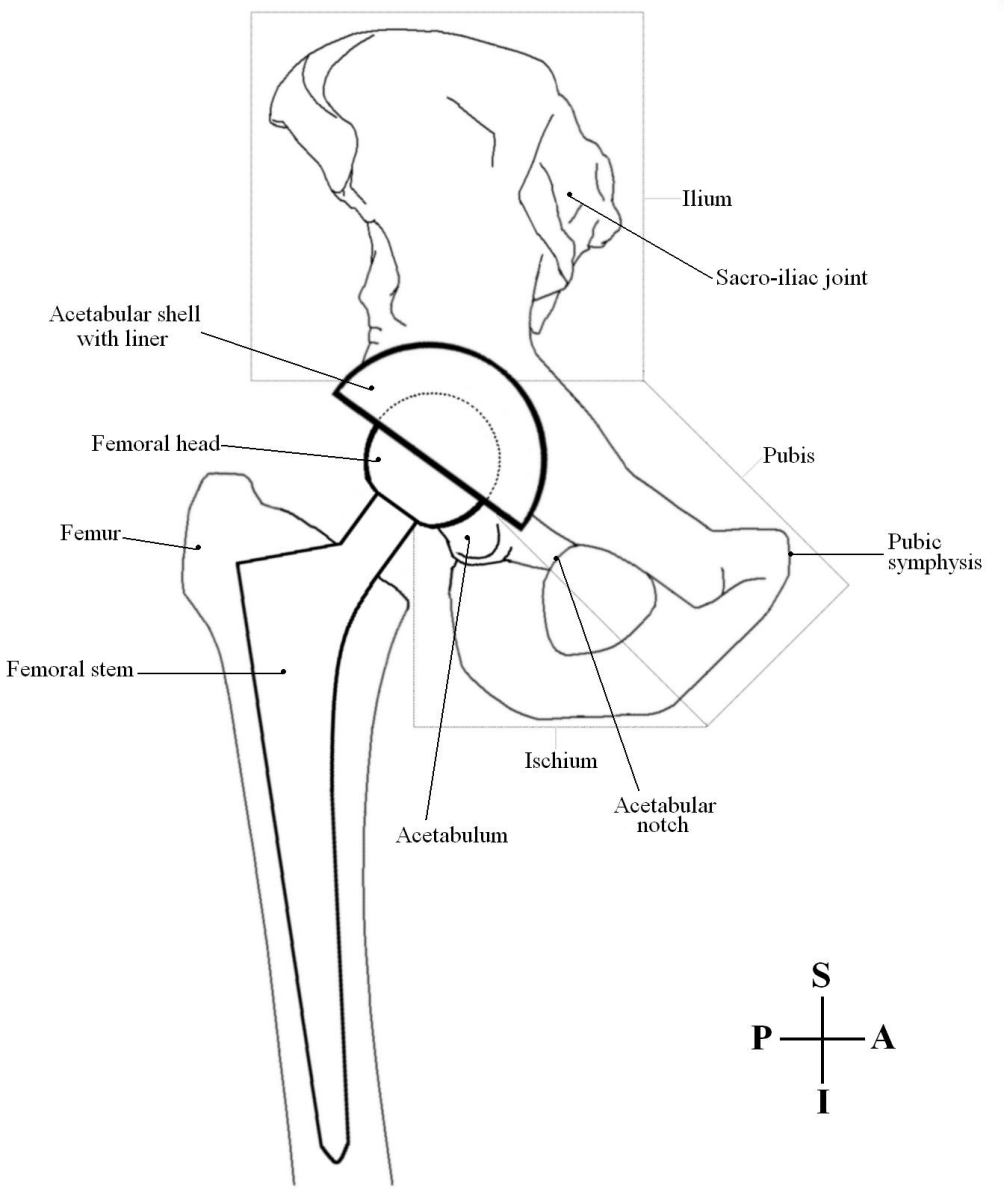

Figure 1: Implanted Total Hip Prosthesis
The hemi-pelvis consists of three fused bones: the Ilium, Pubis, and Ischium. Other anatomical regions that are referenced in this thesis are also depicted. The anatomical directions, S, I, A, P, correspond to Superior (above), Inferior (below), Anterior (before), and Posterior (behind), respectively.

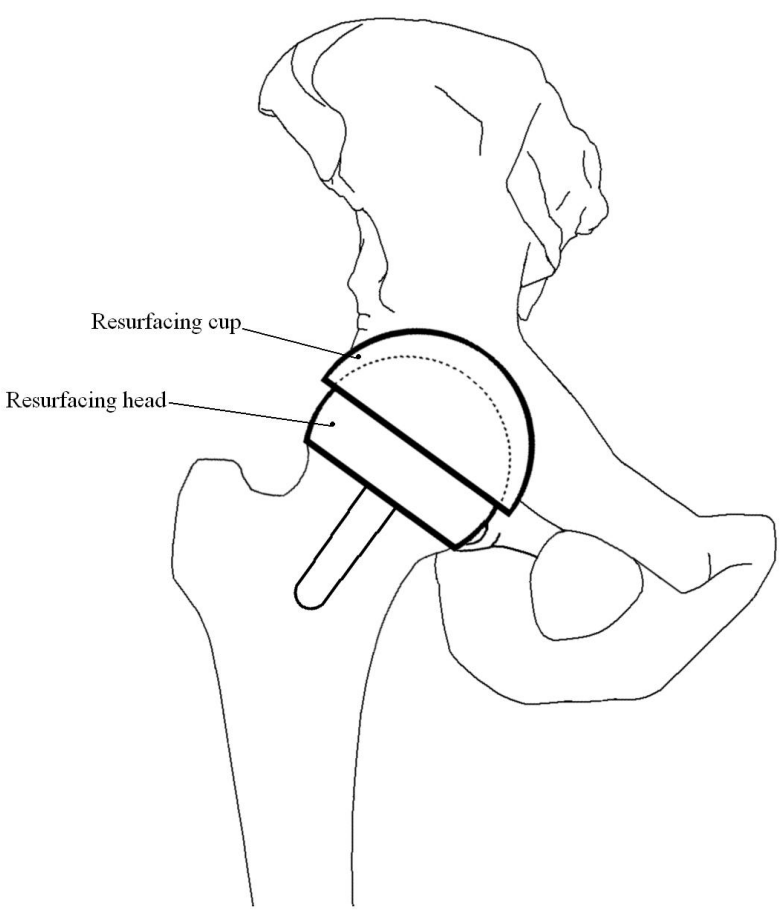

Figure 2: Implanted Hip Resurfacing Prosthesis

The hip resurfacing prosthesis is touted as an attractive alternative to the total hip for younger patients because it requires less bone removal, and it allows for a greater range of motion (Ebied and Journeaux 2003). The metal-on-metal hip resurfacing prosthesis was introduced in 1967 by Maurice Muller and it had promising early clinical results. Unfortunately, it was abandoned in favour of metal-on-plastic prosthetics and did not re-appear until 1988 (Roberts et al. 2005). At the time of writing, the major orthopaedic implant manufacturers offer metal-on-metal hip resurfacing prostheses, although the total

hip remains the prosthesis of choice among clinicians. Worldwide, hip resurfacing prostheses comprise only 6-9% of all implanted hip prostheses. In Canada, this number is 2.7% (CIHI 2009; Huo et al. 2008; Roberts et al. 2005).

Finite element analysis (FEA) is a numerical modeling tool that is used in a wide range of engineering fields including structural analysis, heat transfer, fluid flow, mass transport, and electromagnetic potential. For the sake of brevity and relevance to this thesis, this overview of FEA is presented from a structural engineering perspective. FEA is used to solve problems for which analytical solutions (i.e., mathematical expressions) cannot be obtained. Although analytical solutions provide exact values of desired unknown quantities (e.g., displacement, stress) at any location in the body being analyzed, they are limited in their utility because they can only be obtained for specific, typically simplified problems. In contrast, FEA can be applied to a broad range of complex engineering problems because it uses discretization. Discretization involves subdividing the body into a system of small regions called finite elements, which are interconnected at common locations called nodes. Solutions are then formulated for each element and combined in a 'bottom-up' approach to obtain the solution for the entire body. Each element-level solution is determined via approximation of the displacement at each node with a displacement function that is typically polynomials in form. Consequently, FEA solutions provide approximate values at a discrete number of points in the body (Desai and Abel 1972; Logan 2002).

Finite element modeling consists of three stages: model creation (pre-processing), analysis (processing), and presentation of results (post-processing). Pre-processing consists of four steps. The first step is creation of geometries that represent the bodies being

analyzed. The second step is discretization of relevant geometries into finite elements, a process more commonly known as meshing. Several types of elements are available for use in different types of models. Triangular or quadrilateral elements are typically used in two-dimensional geometries, while tetrahedral, triangular prism (wedge), or hexahedral (brick) elements are used in three-dimensional geometries. Common forms of elements include linear or quadratic. Quadratic elements use second-order polynomial displacement functions (i.e., they have mid-side nodes) and are therefore less stiff and more accurate than equally-sized linear elements, but they are more computationally expensive. The third step is the assignment of material properties. The geometries are assigned material-specific stress-strain curves, thereby providing measures of stiffness on which to base the force-displacement relationships. The fourth step is the application of boundary conditions, which are the physical inputs to the model. The geometries are subjected to known or assumed loads and/or displacements, and are fixed via kinematic constraints so that rigid body motion (i.e., 'flying away') does not occur (Adams and Askenazi 1999; Desai and Abel 1972; Zienkiewicz et al. 2005).

Once creation of the model is complete, matrix equations are set up by the software processor and calculations are performed in the processing stage. If the analysis successfully calculates an accurate solution to the problem as defined in the created model, the analysis is said to be well-conditioned, otherwise it is ill-conditioned. An analysis is ill-conditioned if the model has been set up such that the software's matrix equations cannot be solved accurately, caused by poorly shaped mesh elements, or singular boundary conditions, for example. After a solution is obtained, specified results of interest are generated and presented in formats such as contour or x-y plots during the post-processing

stage. After the results are generated, the next step is to establish the credibility of such results (Adams and Askenazi 1999; Simulia 2007; Yew et al. 2006).

A vital part of finite element modeling is the establishment of model accuracy via the processes of verification and validation. Verification is performed to ensure that the mathematical models of a finite element model are correctly implemented. This involves both code verification and calculation verification. Code verification is performed by FEA software developers and involves comparing benchmark problem solutions generated by the code's algorithms to corresponding analytical, semi-analytical, or highly accurate numerical solutions. Calculation verification typically involves mesh convergence testing to minimize the discretization error of each finite element model. Discretization error can be significant if the mesh consists of too few elements (i.e., the mesh is too coarse), such that the corresponding displacement functions do not yield accurate solutions. Analysis convergence testing minimizes discretization error by generating several meshes with increasing numbers of elements until the results of interest (e.g., displacement, total strain energy, stress, etc.) do not change significantly (i.e., the results have converged). Validation is performed to assess modeling error by determining how closely the finite element model represents the actual system being modeled. Modeling error arises from inconsistencies between the model and the actual system due to assumptions made in geometry, material properties, and boundary conditions. The effect of such inconsistencies on model accuracy can be assessed via validation, which involves comparing the finite element model results to experimental measurements. Validation should be performed after model verification so that mathematical errors are isolated from modeling errors (Anderson et al. 2007; Beaupré and Carter 1992; Desai and Abel 1972).

1.2 Statement of the problem

Concerns exist in the orthopaedic community regarding possible deformation of the resurfacing cup during the surgical procedure of press-fitting (Burnell 2007; Ong et al. 2008). During press-fitting, the surgeon implants the resurfacing cup into the acetabulum, which has been reamed of cartilage and subchondral bone to a diameter 1-2 mm less than that of the cup, by striking an attached impactor several times with a mallet. Post insertion the cup is fixed in place via compressive and frictional forces due to the difference in diameters, or diametral interference. Long term fixation is achieved via growth of cancellous bone into the porous backing of the resurfacing cup (Amirouche et al. 2006; Burnell 2007; Schmalzried and Harris 1992; Shimmin et al. 2008). Unfortunately, such compressive forces deform the resurfacing cup. Since the difference in diameters between the resurfacing head and cup (i.e., diametral clearance) is only 80 – 120 μm, deformation could adversely affect the fluid-film lubrication regime, resulting in compromised implant performance in terms of increased wear (i.e., increased metal ion generation), acoustic emissions, and joint binding (Jin et al. 2006; Langton et al. 2008; Ong et al. 2008; Shimmin et al. 2008).

Resurfacing cup deformation has been studied in experiments with cadavers, foam models, and with FEA (Jin et al. 2006; Udofia et al. 2007; Yew et al. 2006). Experimental studies of resurfacing cup deformation are limited in that cadaver pelvises and resurfacing cups are expensive (Jin et al. 2006). Previous FEA studies were limited in regards to model creation and characterization of cup deformation. The FEA models consisted of simplifying assumptions that may have compromised model validity. A striking example

of this, as described in Chapter 2, is the simple three-dimensional geometry Yew et al. (2006) used to represent a reamed hemi-pelvis. Cup and bone material properties were also assumed to be linear elastic, without consideration of yield behaviour. In addition, cup deformation was not fully characterized in three-dimensions, as deformation was only reported in terms of diametral deformation (i.e., the change in distance between two opposing points) at specified locations around the rim of the cup. Diametral deformation may be insufficient for thoroughly understanding cup deformation, especially in more complex anatomically accurate models. For example, a three-dimensional characterization of cup deformation may be necessary to understand and research the implications of cup deformation on wear (Ebied and Journeaux 2003).

1.3 Objectives

The first objective of this thesis was to create a finite element model of resurfacing cup deformation that addressed deficiencies of previous models in the aspects of pelvic geometry, meshing, cup and bone material properties, and cup insertion (i.e., boundary conditions). The second objective was to demonstrate that diametral deformation measurements at the cup rim are insufficient, by more fully characterizing cup deformation in three-dimensions.

1.4 Thesis layout

This thesis consists of five chapters. Chapter 2 contains a literature review and explores previous finite element studies of resurfacing cup deformation to identify modeling defi-

ciencies, and establishes means of addressing such deficiencies in the 3D model of this thesis. Subsequently, Chapter 3 contains the methodology of this thesis and describes in detail the creation of the 2D axisymmetric and 3D models. Chapter 4 presents and discusses key results generated by the 2D axisymmetric and 3D analyses. This thesis concludes and provides recommendations for future work in Chapter 5.

Chapter 2

Literature Review

This chapter begins with an overview of previous studies that have investigated resurfacing cup deformation. This is followed by a critical assessment of the methodologies employed in the FEA studies to identify deficiencies, and to establish a methodology for the creation of a finite element model that addresses such deficiencies.

Hip resurfacing cup deformation was first investigated experimentally in cadaver pelvises and foam models by Jin et al. (2006). The experimental study used two prototype DePuy ASR^{TM} (DePuy Orthopaedics, Inc., Warsaw, IN) hip resurfacing cups of 60 mm diameter. The first was a thin walled cup (2.3 mm at the equator and 4 mm at the pole) and the second had 'stiffened' walls (3.5 mm at the equator and 6 mm at the pole). Both types of cups were press-fit into cadaver pelvises using a nominal interference of 1 mm, but the actual interference averaged 0.5 mm due to variations in hand-reaming. The authors observed that the cups exhibited compressive deformation predominantly at the ilial and ischial columns (i.e., the superior-anterior acetabular rim at the ilium and the inferior-posterior rim at the ischium). This observation agreed with previous pressure-sensitive film experiments, wherein the compressive forces on two types of press-fit cups were

predominant between the ischial and ilial columns (Widmer et al. 2002). Jin et al. (2006) created a foam model geometry to simulate this cup pinching (see Figure 3), and compared cup deformation results therein to those of the cadaver tests. The maximum diametral deformations observed in the cadaver tests were 63 μm in the thin-walled cups (average 50 μm), and 22 μm in the stiffened cups (average 20 μm). The foam model experiments showed good agreement with cadaver tests at 0.5 mm interference. Specifically, the maximum diametral deformations in the thin-walled and stiffened cups were approximately 55 μm and 30 μm, respectively. In addition, a femoral head with a nominal diametral mismatch of 100 μm was observed to articulate smoothly within the deformed cups in both the cadaver and foam tests.

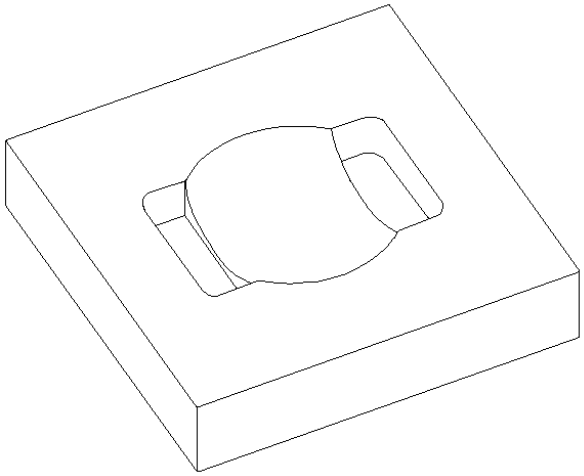

Figure 3: Foam Model Geometry
Representation of the simple 'two-point pinching' geometry of Jin et al. (2006). The two openings adjacent to the acetabular cavity serve to reproduce the ilial-ischial cup compression observed in cadaver tests. This geometry was subsequently used in an FEA study conducted by Yew et al. (2006).

A follow-up FEA study was performed by Yew et al. (2006) to investigate the effects of cup wall thickness, cup size, and interference on hip resurfacing cup deformation in

the foam model geometry. This was done by including a 'thick' DePuy ASR™ (DePuy Orthopaedics, Inc., Warsaw, IN) cup that was available on the market at the time of publication (4.6 mm wall thickness at the equator and 7.9 mm thickness at the pole) in addition to the thin and stiffened (intermediate) cups of Jin et al. (2006). Also, different cup sizes ranging from 46 – 70 mm were used. Yew et al. (2006) showed that for the 60 mm cup having an interference of 0.5 mm, maximum diametral deformations were 120 μm, 43 μm, and 17 μm in thin, intermediate, and thick cups, respectively. These results were not entirely consistent with the corresponding experimental tests conducted by Jin et al. (2006). Although the maximum diametral deformation differed by only 13 μm in the stiffened cup, the deformation was overestimated by 65 μm in the thin cup.

Udofia et al. (2007) also presented a finite element analysis of hip resurfacing cup deformation, although the majority of their study focused on the micromotion and contact pressure between the resurfacing cup and acetabulum under simulated mid to terminal stance loading of the gait cycle. Udofia et al. (2007) examined a conceptual design of a 58 mm diameter Durom™ (Zimmer, Warsaw, IN) resurfacing cup, with uniform wall thickness of 4 mm, under press-fitting configurations of 1 and 2 mm diametral interferences. Diametral deformation of the seated cup was determined in the anteroposterior and superoinferior directions at the rim of the resurfacing cup. For the cup press-fit with 1 mm of interference, Udofia et al.(2007) reported cup deformations of 24 μm and 49 μm in the anteroposterior and superoinferior directions, respectively.

In the finite element models of Yew et al. (2006) and Udofia et al. (2007), there were deficiencies regarding pelvic geometry and measurement of resurfacing cup deformation. In the study of Yew et al. (2006), the complex geometry of the hemi-pelvis was repre-

sented by a simple 3D (foam model) geometry (see Figure 3). Cup deformation was symmetric due to the symmetry of the simple 3D geometry, and was measured via diametral deformation at the rim. In reality, cup deformation is expected to be highly irregular, and measurement of diametral deformation at the rim of the cup may not be sufficient for describing cup deformation; full deformation characterization in 3D that provides a measure of cup asphericity may be necessary. Udofia et al. (2007) used an anatomically accurate geometry, but unfortunately they too reported only diametral deformation at the cup rim. Three-dimensional cup deformation has important implications on wear, as *in vitro* wear simulations have shown that the main contributor to wear is head and cup asphericity (Ebied and Journeaux 2003). This thesis addresses this issue by using an anatomically accurate 3D geometry for modeling of resurfacing cup deformation, and by exploring a means of characterizing cup deformation in 3D.

Regarding meshing, deficiencies were present in the model of Udofia et al. (2007). The cortical bone was not geometrically delineated but specified with a layer of shell elements. Shell elements of a specified thickness are used on the surface of the pelvic geometry in lieu of creating a thin cortical bone layer and meshing with continuum (solid) elements in order to avoid element distortion in the thin cortical bone layer (Phillips et al. 2006). Unfortunately, there may be problems with the solution accuracy when combining the shell elements of the cortical bone with the continuum elements of the cancellous bone. The combination of shell elements with continuum elements may yield inaccurate results, given that shell elements have three translational (u_x, u_y, u_z) and three rotational (φ_x, φ_y, φ_z) degrees of freedom at each node, but continuum elements have only three translational degrees of freedom at each node (Beevers et al. 2001; Shim et al.

2002). When shell elements are attached to continuum elements, the rotations in the shell elements cannot be transferred properly to the continuum elements, causing potential problems with solution accuracy. This thesis avoids such issues by geometrically defining a uniform layer of cortical bone in the anatomically accurate geometry and meshing the entire geometry with continuum elements.

Deficiencies were also present with material properties in the studies of both Yew et al. (2006) and Udofia et al. (2007). Yew et al. (2006) and Udofia et al. (2007) assumed the CoCr cup and pelvic bone to be linearly elastic, but this does not allow for the possibility of both materials exhibiting yield behaviour during press-fitting. The inclusion of yield behaviour is necessary to determine if the cup and bone may permanently deform during press-fitting. This thesis addresses this issue by including yield behaviour for the cup and bone. Regarding linear elasticity of bone, a Young's modulus and Poisson's ratio of 17 or 18 GPa and 0.3, respectively, are typically used for cortical bone in finite element studies (Anderson et al. 2005; Ong et al. 2006; Bellini et al. 2007). These values are based on data obtained from the human femur or tibia, as no data on pelvic bone is available. Yew et al. (2006) and Udofia et al. (2007) assumed a Young's modulus of 17 GPa and a Poisson's ratio of 0.3.

For cancellous bone, several studies have derived heterogeneous Young's modulus values via density-modulus relationships obtained from Computed Tomography (CT) (Anderson et al. 2005; Dalstra et al. 1995; Ong et al. 2006); others have assumed a constant value throughout the pelvis (Bellini et al. 2007; Spears et al. 2001; Udofia et al. 2007). Yew et al. (2006) assumed a Young's modulus of 800 MPa and Udofia et al. (2007) assumed a value of 500 MPa, each with a Poisson's ratio of 0.3. Other finite ele-

ment studies pertaining to the pelvis have used values as low as 100 MPa and 0.2, respectively, based on a landmark study of the mechanical and textural properties of pelvic cancellous bone conducted by Dalstra et al. (1993) (Bellini et al. 2007; Dalstra et al. 1993; Spears et al. 2001). In this study, Dalstra and co-workers (1993) found that the Young's modulus rarely exceeded 100 MPa, and determined the Poisson's ratio to be 0.2. Also, Dalstra et al. (1993) discovered that cancellous bone exhibits little anisotropy, and as a result, some researchers have concluded that modeling cancellous bone as isotropic is a reasonable assumption (Phillips et al. 2006; Bellini et al. 2007).

Deficiencies were also present in the press-fitting simulations of both Yew et al. (2006) and Udofia et al. (2007). Prior to conducting their 3D FEA simulations, Yew et al. (2006) tested two different press-fitting methods using a 2D axisymmetric pelvic geometry to determine which was most appropriate for use in their 3D model. The 2D axisymmetric geometry consisted of a cross-section of the ilium and acetabulum that, when rotated 360˚ about an axis of symmetry through the pole of the acetabulum, yielded a three-dimensional representation of the acetabulum and surrounding pelvic bone (Spears et al. 1999). A representation of the 2D cross-section is shown in Figure 4.

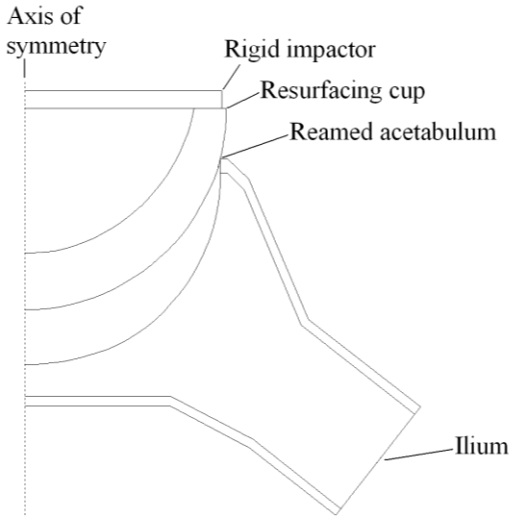

Figure 4: 2D Axisymmetric Geometry
Representation of the two-dimensional axisymmetric geometry used by Yew et al. (2006) in their simulation of press-fitting of resurfacing cups.

The two press-fitting methods that were tested included the multiple-displacement (MD) and multiple-load (ML) methods (Yew et al. 2006). The MD method simulates multiple mallet impacts via a series of increasing impactor displacements applied to the cup. The first impact is simulated by applying a displacement equivalent to the initial distance between the pole of the cup and the floor of the acetabulum (i.e., the polar gap), after which the cup is allowed to rebound by deactivating the impactor displacement. Subsequent impacts are simulated by increasing the displacement by 1 mm for each additional impact until the cup does not penetrate any further into the acetabulum (i.e., the polar gap no longer decreases). Also, if during impact divergence of solution occurs, the displacement is decreased by 0.5 mm and the analysis is rerun to obtain solution convergence. In the ML method, loads are applied to the cup via an impactor. The initial load is obtained

from the force data output by the corresponding MD analysis, and each subsequent impact increases the force by a factor of 1.5 until the analysis diverges.

Yew et al. (2006) ultimately chose to use the MD method in their 3D model because it "usually" required less computational time, in spite of their views that the ML method was more realistic. Yew and co-workers (2006) noticed that the force on the impactor corresponding to the initial displacement in their MD model was "an unrealistically high load of 100kN." This load was deemed to be unrealistic in comparison to the press-fitting loads used by Spears et al. (1999), since the maximum load used in that study was only 4 kN. Yew et al. (2006) conjectured that one of the reasons why that the load was so high was due to the use of one large initial displacement instead of several incremental displacements (this was done to reduce the number of impacts, and therefore computational time). Unfortunately, Yew et al. (2006) did not investigate this. Also, the rationale behind Yew et al.'s (2006) statement that the ML method was more realistic is not clear, as the initial impact force in the ML model was obtained from the output of the MD model, and the polar gap and cup deformation results between the two methods were in agreement. This thesis addresses these discrepancies via 2D axisymmetric analyses, in order to determine the most suitable press-fitting method to use in the anatomically accurate 3D model of this thesis. The 2D axisymmetric analyses are used for this purpose because analysis runtimes are much faster compared to 3D analysis runtimes (minutes compared to days).

Udofia et al. (2007) simulated press-fitting via the interference fit method instead of using a displacement or force method. The interference fit method consists of positioning the resurfacing cup in the fully seated position in the acetabulum and realigning the over-

lapping cup-acetabulum surface nodes. This method is easy to employ and is computationally inexpensive, but it may not be appropriate for studying cup deformation because the physical process of press-fitting is not considered; the mallet impacts and rebounding of the cup after each impact are not taken into account.

During press-fitting, Udofia et al. (2007) fully constrained the sacro-iliac and pubic symphysis joints, as done in previous finite element studies that have used anatomically accurate pelvic geometries (Spears et al. 2000; Spears et al. 2001). Bellini et al. (2007) suggested that fully constraining these joints may not allow true pelvic bone response to external loading. In their finite element study of the effect of post-operative weight bearing on implant stability, Bellini et al. (2007) allowed relative translation at the interfaces of these two joints in the superior-inferior direction to simulate sacral and pubic support. A recent finite element study by Phillips et al. (2007) supports the boundary condition argument of Bellini et al. (2007). Phillips et al. (2007) compared the effect of fixed versus spring-simulated muscle and ligament boundary conditions on the stress and strain distributions in a single leg stance pelvis model. Phillips et al. (2007) found that stress was reduced and distributed more evenly throughout the pelvic bone in the model with muscle and ligament boundary conditions compared to the model with fixed boundary conditions. Phillips et al. (2007) did observe similar stresses in the acetabular region between the two models, however, and suggested that the use of fixed constraints may suffice for studies pertaining to this region.

Chapter 3

Methodology

This chapter describes the methodology used in this thesis to create finite element models of press-fitting of a resurfacing cup. Included in this description are details about the creation and meshing of the geometries, the assignment of mechanical properties, and the simulation of cup insertion. First, geometries were created via laser scanning and CAD modeling, and consisted of both two- and three-dimensional representations of a reamed hemi-pelvis, a resurfacing cup, and an impactor. Laser scanning was used to obtain the hemi-pelvis geometry because it was a cost-effective alternative to using Computed Tomography to obtain a geometry that was closely representative of an actual geometry (i.e., anatomically accurate). Meshing was then performed on the pelvic and cup geometries using linear elements; different mesh densities were used for convergence testing and element distortion was reduced in every mesh. Material properties and contact behaviour assumptions were assigned to the pelvic bone, resurfacing cup, and impactor. Finally, the simulation of cup insertion involved initial cup placement followed by press-fitting using prescribed boundary conditions.

3.1 Creation of model geometries

Two-dimensional (2D) axisymmetric and three-dimensional (3D) finite element models were created using geometric representations of a surgically prepared (i.e., reamed) hemi-pelvis, resurfacing cup, and an impactor. The 2D axisymmetric model uses a simple representation of a reamed hemi-pelvis to determine the most appropriate simulated press-fitting method to use in the 3D model; the 3D model could not be used because it is more computationally expensive (i.e., analysis runtimes that take days instead of minutes). The 3D model uses an anatomically accurate representation of a reamed hemi-pelvis to investigate the magnitude and mode of deformation of a press-fit resurfacing cup. This section describes the methodologies used to create 2D and 3D pelvic geometries, and provides the specifications used for the resurfacing cup and impactor geometries.

The reamed hemi-pelvis geometry used in the anatomically accurate 3D model of this thesis consists of a 2 mm uniformly thick cortical bone layer that surrounds a cancellous bone region, with a reamed acetabulum. A 2 mm thickness was chosen for the cortical layer because previous studies have assumed 1-2 mm cortical bone thickness, and 2 mm would avoid any potential element distortion problems associated with a 1 mm thickness (Phillips et al. 2007). This geometry was created by laser scanning a large plastic SAW-BONES® right hemi-pelvis replica with a 57 mm acetabulum (item no. 1297-1) (Pacific Research Laboratories, Vashon, Washington) and digital post-processing of the scanned data. The exterior surface geometry of the hemi-pelvis was obtained with the use of a ShapeGrabber® 3D Laser Scanner (ShapeGrabber, Ottawa, Ontario) with 0.2 mm scanning accuracy. Three-dimensional point cloud datasets representing different orientations

of the surface of the hemi-pelvis replica were obtained and registered together in Geomagic Studio® reverse engineering software (Geomagic, Research Triangle Park, NC) to within an average distance of 58 μm (SD: 80 μm) of one another, forming a point cloud sampling of the hemi-pelvis' continuous surface. The resulting point cloud was subsequently converted into a triangulated polygonal surface to within an accuracy of 25 μm of the point cloud, and then converted to a NURBS (Non-Uniform Rational B-Spline) exterior surface geometry that was within an average of 2 μm (SD: 27 μm) from the polygonal surface, for import into ABAQUS. Figure 5 shows the resulting NURBS exterior surface geometry of the hemi-pelvis.

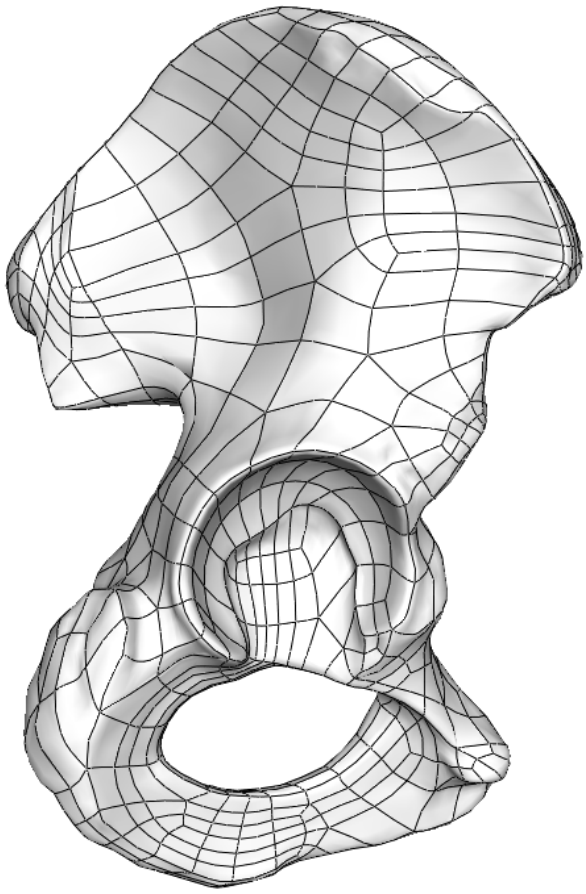

Figure 5: NURBS Exterior Surface Geometry of the Hemi-Pelvis

The cortical and cancellous bone regions of the hemi-pelvis geometry were defined by creating a cortical/cancellous boundary geometry and merging it with the exterior surface geometry of the hemi-pelvis. The geometry of the cortical/cancellous boundary was created by first offsetting the triangulated exterior surface of the hemi-pelvis 2 mm to its interior using the surface offset procedure in Geomagic Studio, and then digitally processing the offset geometry. This digital processing involved the manual removal of intersecting triangles (as detected by the software) and corners that appeared to be non-

smooth (i.e., jagged, or sharp in appearance), as well as removal of the acetabular fossa, in order to eliminate ill-defined (i.e., less than 0.1 mm in thickness) volumes that cannot be meshed. As with the exterior surface geometry of the hemi-pelvis, the resulting triangulated cortical/cancellous boundary surface geometry was converted to a NURBS surface and imported into ABAQUS. The geometry is shown in Figure 6.

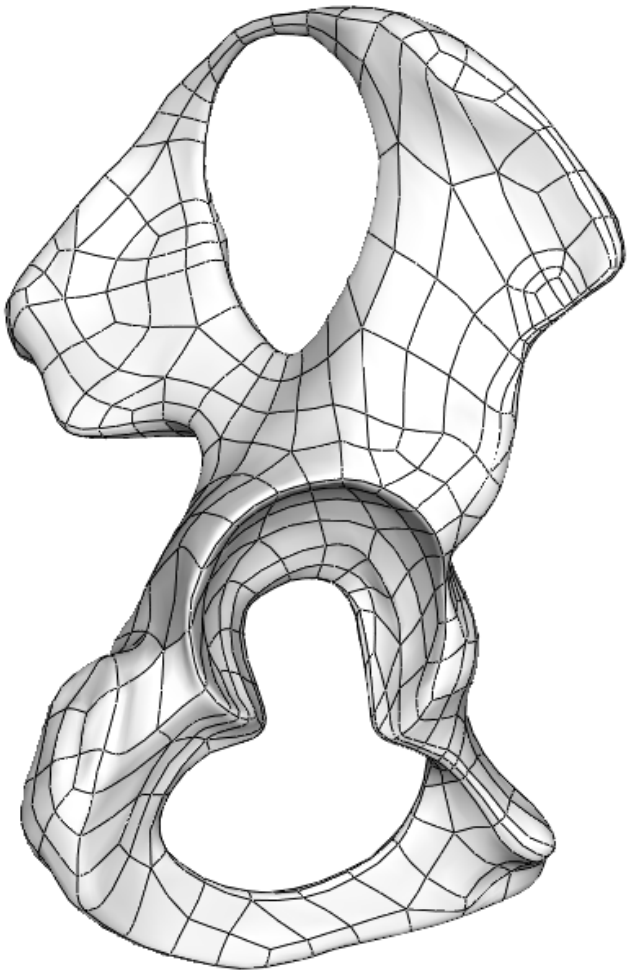

Figure 6: NURBS Cortical/Cancellous Boundary Surface Geometry

The reaming of the acetabulum was simulated by subtracting a sphere from the acetabular region of each of the exterior and cortical/cancellous boundary surface geome-

tries of the hemi-pelvis (Bellini et al. 2007), and then merging the reamed geometries together to produce the reamed hemi-pelvis geometry. In Geomagic Studio, a sphere was fit to the lunate surface of the acetabulum (i.e., inner surface, excluding the floor) in the exterior surface geometry of the hemi-pelvis to obtain the centre and diameter of the acetabulum. The size of the reaming sphere was determined by taking into consideration that the sphere had to be at least 4 mm larger in diameter than that of the best-fit sphere in order to completely remove the cortical bone when subtracted from the acetabulum (i.e., the 2 mm of cortical bone on opposite sides of the sphere would be removed). Also taken into consideration was that an approximate interference fit of 1 mm for a given cup size had to be created. The diameter of the best-fit sphere was measured in Geomagic Studio to be 55.8 mm, and as such, a reaming sphere of at least 60 mm in diameter was required; but given that the available cup sizes were 60, 62, 64, and 66 mm, a 62 mm cup (outer diameter = 62.6 mm) dictated a spherical reaming diameter of 61.6 mm to achieve a 1 mm interference.

The 61.6 mm diameter sphere was created and positioned in ABAQUS, such that its centre coincided with the centre of the best-fit sphere. The 61.6 mm sphere was initially subtracted from each of the exterior and cortical/cancellous boundary geometries, but the cortical bone region near the floor of the acetabulum in the merged hemi-pelvis geometry was too thin (i.e., less than 0.1 mm thick) to mesh without element distortion. The reaming sphere was then iteratively repositioned and subtracted to find a suitable reaming configuration. Repositioning of the sphere involved its translation towards the acetabulum along the line normal to a plane on the acetabular rim and through the centre of the best-fit sphere by increments of 0.1 mm (the definition of the acetabular plane is described in

the next paragraph, which details the creation of the 2D axisymmetric geometry). Unfortunately, no suitable position was found using this method with this size of reaming sphere because regions with thin cortical bone could not be completely eliminated. Another reaming configuration was then attempted by creating a reaming sphere with a 63.6 mm diameter that corresponded to a 64 mm cup (o.d. = 64.6 mm) with an interference of 1 mm. Again, excessively thin cortical bone regions were present in the initial merged hemi-pelvis geometry, so the same iterative translation-subtraction methodology was used to attempt to find a suitable reaming configuration. Ultimately, reaming of the acetabulum without introducing excessively thin cortical bone was achieved by translating the 63.6 mm diameter sphere 2 mm and subtracting it from the acetabulum. Any small faces created during the reaming procedure were repaired (i.e., removed) in order to avoid associated meshing difficulties. Figure 7 depicts the reamed hemi-pelvis geometry.

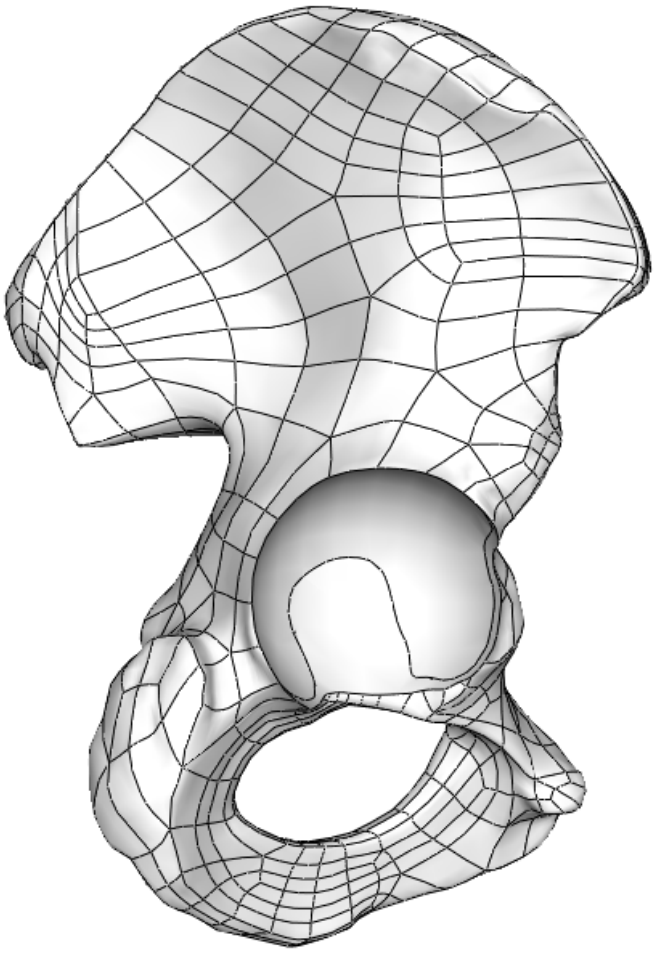

Figure 7: Reamed Hemi-Pelvis Geometry

The 2D axisymmetric geometry was derived from measurements taken of a cross-section through the acetabulum of the reamed hemi-pelvis geometry. Prior to cross-sectioning, an acetabular rim plane was created via three points defined on the exterior surface (i.e., unreamed) geometry of the hemi-pelvis (Figure 8). The normal to the resulting plane served as an axis of symmetry in the final 2D axisymmetric model. The cross-section itself was obtained via a partitioning plane in ABAQUS, which was defined by selecting three points on the reamed hemi-pelvis geometry (Figure 9). The points were

chosen such that the resulting plane yielded a cross-section through the centre of the acetabulum (as defined by the best-fit sphere), and through a thin section of the acetabular wall. After cross-sectioning, a line orthogonal to the acetabular rim plane – the axis of symmetry – was specified through the centre of the acetabulum (Figure 10). A 2D axisymmetric geometry was sketched on the cross-section by approximating the geometry with straight lines. The dimensions and angles necessary for creation of the 2D axisymmetric geometry were obtained, and are depicted in Figure 11. The following figures summarize the process of obtaining the 2D axisymmetric measurements.

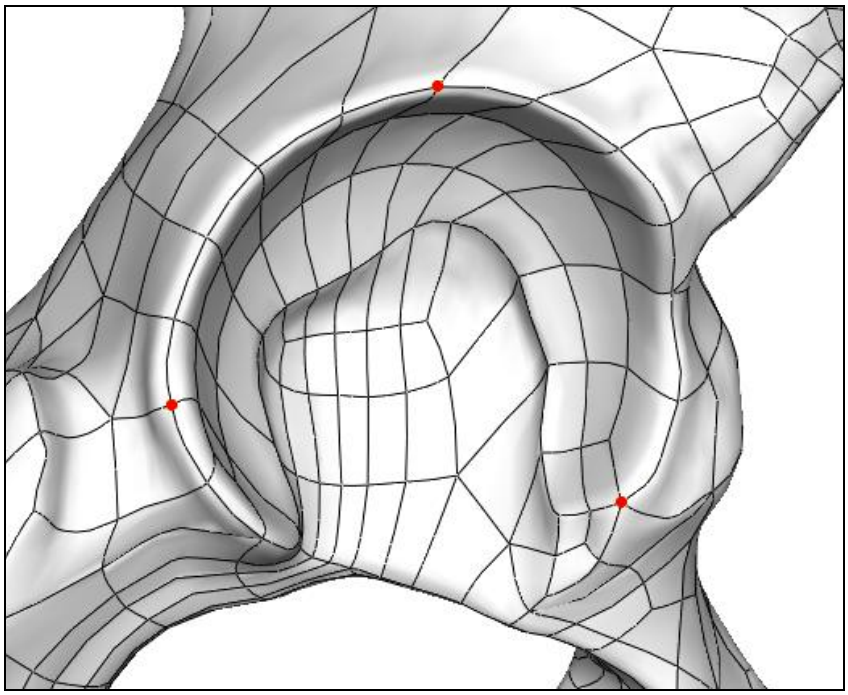

Figure 8: Three Acetabular Rim Points for Plane Fitting

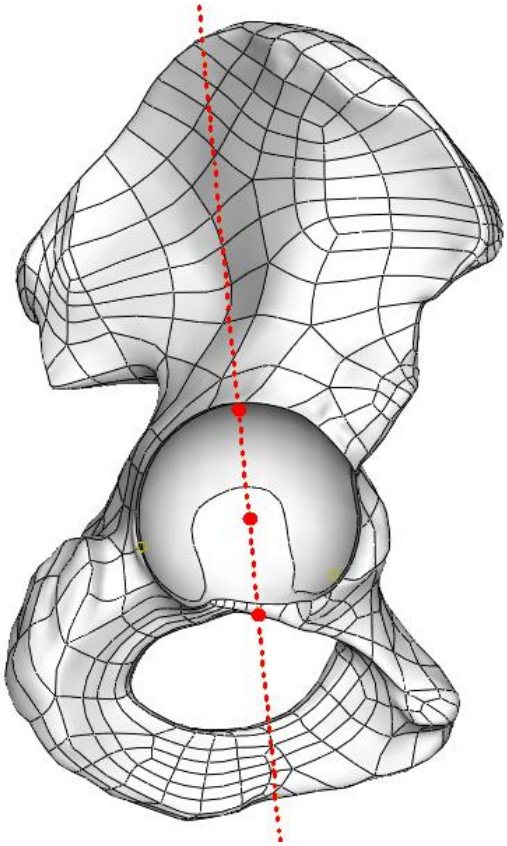

Figure 9: Three Points for Acetabular Cross-Sectioning

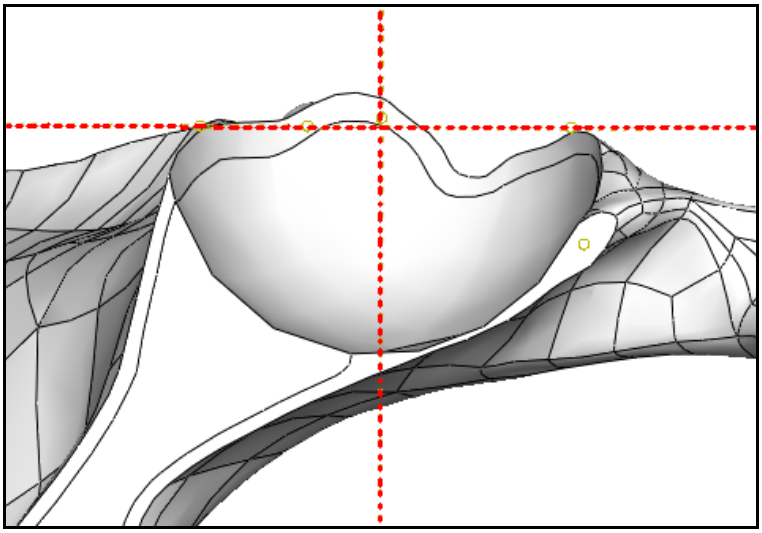

Figure 10: Acetabular Cross-Section
Cross-section through the acetabulum of the reamed hemi-pelvis geometry, with the acetabular rim plane (horizontal line) and axis of symmetry (vertical line) shown.

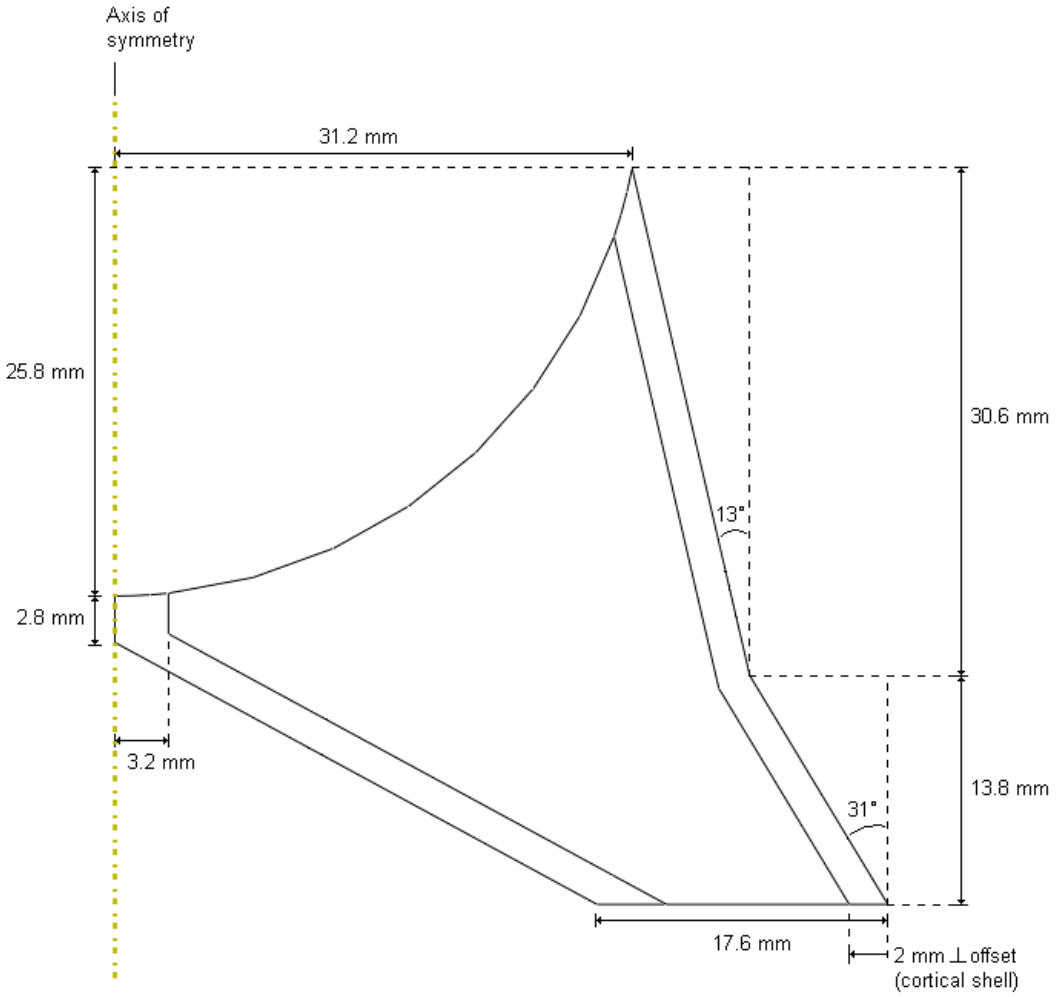

Figure 11: 2D Axisymmetric Geometry Measurements

A Birmingham Hip™ (Smith & Nephew, Memphis, Tennessee) resurfacing cup is modeled in this thesis. As discussed earlier, a cup size of 64 mm was chosen because this size was amenable to a suitable reaming configuration. The cup geometry is based on measurements taken from an x-ray template, and was created with the native pre-processor CAD tools in ABAQUS/CAE. The 1 mm thick CoCr bead coating on the exte-

rior of the cup was ignored, in that it was assumed to be solid CoCr throughout as was done in previous works (Udofia et al. 2007; Yew et al. 2006). The dimensions of the 64 mm resurfacing cup are shown in Figure 12.

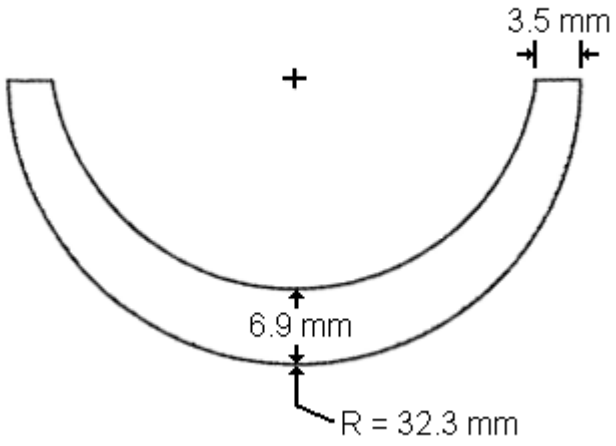

Figure 12: Dimensions of the 64 mm Birmingham Hip™ Resurfacing Cup

The impactor was simulated in this thesis by an analytically rigid circular plate geometry with a radius of 31.8 mm, 0.5 less than the outer radius of the resurfacing cup. A flush or overhanging radius was not specified in order to avoid potential problems associated with physical interference of the impactor with the rim of the acetabulum during press-fitting.

3.2 Meshing

This section describes element selection, meshing for convergence testing, and mesh verification of the 2D axisymmetric and 3D finite element geometries. The types of ele-

ments used were selected based on the geometric, contact, computational efficiency considerations. The computational accuracy of the finite element models was verified via convergence testing, which involved successive mesh refinements until the results of interest did not change significantly. Distorted elements were identified via mesh verification checks that used specific distortion criteria including shape factor, small and large face corner angles, and aspect ratio. Distorted elements were eliminated via remeshing to reduce a source of computational error.

Three criteria were used to choose the appropriate element types for meshing the geometries: the ability to mesh the geometries without introducing excessive distortion, amenability to contact analysis, and to computation. In the anatomically accurate 3D model, the resurfacing cup geometry was meshed with linear hexahedral elements (i.e., C3D8R) and the pelvic geometry was meshed with linear tetrahedral elements (i.e., C3D4). Hexahedral elements were chosen because they have good contact analysis capabilities and they are computationally efficient (Simulia 2007). Tetrahedral elements were used because the highly irregular shape of the reamed hemi-pelvis is not conducive to meshing with hexahedral elements. When using tetrahedral elements in contact analyses, ABAQUS recommends the modified quadratic tetrahedral elements (Simulia 2007). Unfortunately, modified quadratic tetrahedral elements could not be used because they proved too computationally expensive, in that analysis times took on the order of weeks, even on a workstation with 8 GB of RAM. In the 2D axisymmetric model, the resurfacing cup was meshed with linear quadrilateral elements (i.e., CAX4R), and the pelvic geometry was meshed with linear triangle elements (i.e., CAX3). These elements were chosen to be consistent with the 3D model.

Convergence testing was performed to verify the computational accuracy of the 2D axisymmetric and 3D finite element models. This involved the comparison of results generated from successive mesh refinements, until the results converged to within an acceptable error tolerance. Percent changes in nodal displacements (deflections) and/or total strain energy between successive analyses are typically used as convergence indicators (Luo and Häussler-Combe 2003; Marks and Gardner 1993; Ramos and Simões 2006; Stolk et al. 2001). This thesis used total strain energy to determine when further mesh refinement was no longer required. Each model was considered to be converged when the total strain energy of an analysis relative to the energies of three consecutive analyses were within an error of 2%. The error in total strain energy between analyses was calculated using the formula:

$$\Delta U = \frac{U_N - U_i}{U_i} * 100\% \quad (1)$$

Where U_N is the total strain energy of the current analysis and U_i is the total strain energy of a given previous analysis. The total strain energy was calculated in ABAQUS as total internal energy (output variable: ALLIE).

For convergence testing, the geometries of the 2D axisymmetric and 3D models were meshed using the automatic mesh generator with global seeding, followed by local reseeding to eliminate distorted elements. For each model, several successively refined meshes were created by decreasing the global seed size (average element edge length), thereby increasing the number of elements (and therefore degrees of freedom). Each generated mesh was subjected to mesh verification checks in order to identify overly dis-

torted elements. Verification checks were performed using shape metrics including shape factor, small face corner angle, large face corner angle, and aspect ratio as verification criteria. The criteria limits were derived from the ABAQUS' set defaults (Simulia 2007), and are shown in Table 1 .

Table 1: Shape Metrics Mesh Verification Criteria and Limits

Verification Criterion	Quadrilateral/ Hexahedral	Triangle/ Tetrahedral
Shape factor	N/A	0.01/0.0001
Small face corner angle	10	5
Large face corner angle	160	170
Aspect ratio	10	10

Any elements that did not meet the default limits were eliminated via local mesh refinement. The number of distorted elements was greatly reduced via local mesh refinement, but they could not be completely eliminated. Excessive element distortion did not occur in the 2D axisymmetric meshes, but it occurred predominantly in the acetabular region of the 3D meshes. Local remeshing efforts were concentrated in the acetabulum because it is a critical region in these analyses. Local mesh refinement was performed by manually reseeding the edges of corresponding NURBS faces at a higher density and remeshing. The following tables provide details of the meshes created for each of the 2D axisymmetric and 3D models. Convergence data based on total internal energies from the 3D model is also included.

Table 2: 2D Axisymmetric Model Mesh Densities
The proposed mesh densities for use in the convergence tests of the 2D axisymmetric model. The cup was seeded such that the number of elements across the rim increased by one in each successive analysis (*N.B.* the rim of the cup in analysis 4 required local seeding to achieve five elements across).

Analysis No.	Global Seed No. (mm)		No. of Elements		
	Cup	Pelvis	Cup	Pelvis	Total
1	1.5	3.0	62	211	273
2	1.25	2.0	111	454	565
3	1.0	1.5	184	811	995
4	0.9225	1.0	250	1655	1905
5	0.8	0.75	342	3086	3428
6	0.7	0.6	462	4805	5267
7	0.65	0.5	568	6842	7410

Table 3: 3D Model Mesh Densities
The proposed mesh densities for use in the convergence tests of the 3D model. As in the 2D axisymmetric model, the cup was seeded such that the number of elements across the rim increased by one in each successive analysis.

Analysis No.	Global Seed No. (mm)		Local Seed No. (mm)	No. of Elements			% Distorted Elements Remaining
	Cup	Pelvis	Acetabulum	Cup	Pelvis	Total	
1	1.25	6.0	2.0	12,540	185,745	198,285	0.07
2	1.0	5.0	1.5	26,112	223,937	250,049	0.01
3	0.9	4.0	1.0	40,540	270,471	311,011	0.03
4	0.75	3.0	0.75	70,656	370,568	441,224	0.03
5	0.5	2.0	0.6	182,868	609,871	792,739	0.02

Table 4: 3D Model Convergence Data
Total internal energy at the end of rebound 1 for each analysis in the anatomically accurate model. The greatest absolute difference in total internal energy relative to the third analysis is shown.

Analysis No.	Total Internal Energy (J)	% $\lvert\Delta\rvert_{Max}$
1	4.466	–
2	4.351	–
3	4.434	1.9

3.3 Assignment of mechanical properties

This section defines the material and contact properties assigned to the impactor, resurfacing cup, and pelvic geometries. The material properties include Young's modulus, Poisson's ratio, yield stress, and ultimate strength and strain. Contact properties were chosen to facilitate solution convergence and are based on previous studies and experimental data.

3.3.1 Material properties

The material properties of the resurfacing cup and pelvic bone (the impactor is a rigid surface), were assumed to be homogeneous isotropic linear elastic with strain-hardening after the onset of yielding, such that failure could be estimated via the von Mises criterion. Such an assumption is typically applied for ductile materials such as metals, but it is not very realistic for bone because it assumes equal strength (ultimate stress) in tension and compression. Notwithstanding, this assumption has been used extensively by researchers for estimating bone fracture risk (Doblaré et al. 2004). The von Mises formula:

$$\sqrt{\frac{(\sigma_2-\sigma_3)^2+(\sigma_3-\sigma_1)^2+(\sigma_1-\sigma_2)^2}{2}} = \sigma_y \qquad (2)$$

Where: σ_1, σ_2, σ_3 are the three principal stresses, and

σ_y is the yield stress.

Figure 13 illustrates a stress-strain curve for a linear elastic material with strain-hardening behaviour.

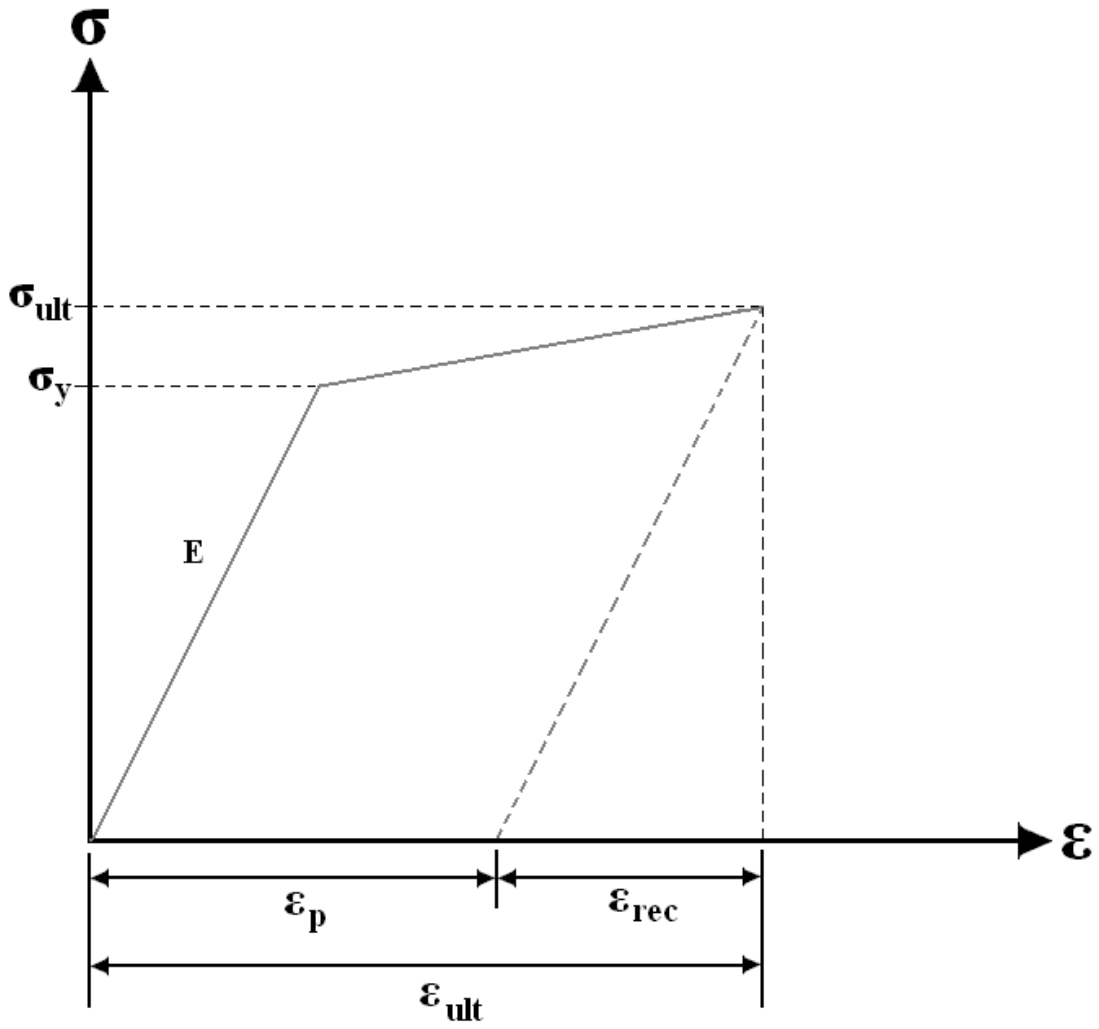

Figure 13: Stress-Strain Curve for a Linear Elastic Material with Strain-Hardening
The stress-strain curve shows that the material with a Young's modulus, E, (slope of the first portion of the curve) exhibits linear elastic (i.e., non-permanent) strain (i.e., deformation) until the yield stress, $\sigma_{y,}$ is reached. Further deformation is elasto-plastic (i.e., permanent), until the ultimate stress, σ_{ult}, is reached, at which point the material fails (i.e., fractures). After fracture, the material recovers elastic strain, ε_{rec}, from the ultimate strain, ε_{ult} (the slope of the recovery line is parallel to the linear elastic portion of the stress-strain curve, and is therefore equal to the Young's modulus, E), with only plastic strain, $\varepsilon_{p,}$ remaining.

The CoCr resurfacing cup was assigned a Young's modulus of 200 GPa, a Poisson's ratio of 0.3, a yield stress of 450 MPa, and an ultimate strength of 655 MPa with 8% elongation (Gilbert 2007; Katz et al. 2004). The material properties of pelvic bone assumed in the finite element models of this thesis are based on experimental data and values used in recent finite element studies of the pelvis. The 2 mm cortical bone layer was assigned a Young's modulus of 17 GPa, a Poisson's ratio of 0.3, a yield stress of 181 MPa, and an ultimate strength of 205 MPa at an ultimate strain of 0.031 (Cezayirlioglu et al. 1985; Udofia et al. 2007; Yew et al. 2006). The cancellous bone was assigned a Young's modulus of 300 MPa, a Poisson's ratio of 0.2, a yield stress of 1.92 MPa, and an ultimate strength of 2.23 MPa at an ultimate strain of 0.0145 (Bellini et al. 2007; Kopperdahl and Keaveny 1998; Spears et al. 2001). In ABAQUS, isotropic hardening of materials is specified via plastic strains. To calculate plastic strain for each material, the following equation is used:

$$\varepsilon_p = \varepsilon_{ult} - \frac{\sigma_{ult}}{E} \tag{3}$$

Where:

ε_p is the plastic strain,

ε_{ult} is the ultimate strain,

σ_{ult} is the ultimate stress, and

E is the Young's modulus.

3.3.2 Contact properties

The contact interactions between the exterior of the resurfacing cup and the acetabulum were based on previous studies and experimental data wherever available. This involved selection of 'master' and 'slave' surfaces, and choice of suitable contact discretization methods, sliding modes, and Coulomb friction models.

The surfaces that are expected to come into contact with one another during a simulation must be specified as contact pairs in ABAQUS. In this study, impactor-cup and cup-acetabulum contact surface pairs were specified. The impactor-cup contact pair consists of the bottom surface of the impactor and the surface of the cup rim; the cup-acetabulum contact pair consists of the exterior of the cup and the acetabular surfaces. In order to model contact between a given contact pair, one surface is designated as the "master" and the other the "slave." Selection of the appropriate surface to act as the master is based on master-slave contact pairing convention. For the impactor-cup contact pair, the impactor surface was specified as the master because an analytically rigid surface must always be the master surface. For the cup-acetabulum contact pair, the cup was specified as the master surface because ABAQUS recommends that the stiffer body in a contact pair be specified as the master surface (and the cup is stiffer than bone) (Simulia 2007).

Each contact pair was required to use one of ABAQUS's two discretization methods: node-to-surface discretization, or surface-to-surface discretization (Simulia 2007). In node-to-surface discretization, contact is defined by the projection of the slave surface nodes onto the master surface. During the analysis, the slave nodes do not penetrate the master surface, but the master surface can penetrate the slave surface. In contrast, sur-

face-to-surface discretization averages contact between the master and slave surfaces, providing more accurate pressure and stress distribution (Simulia 2007). In order to achieve analysis convergence in the finite element models, it was necessary to use node-to-surface discretization in the 2D axisymmetric model, and surface-to-surface discretization in the 3D model. Surface-to-surface discretization could not be used in the 2D axisymmetric model because this resulted excessive overclosure of the contact surfaces, given the relatively small number of nodes involved in contact. Node-to-surface discretization could not be used in the 3D model because this resulted in excessive penetration of the master nodes into the slave surface, given the relatively large number of nodes involved in contact.

The mode of sliding between the surfaces of each contact pair was specified after selecting the discretization method. ABAQUS provides two sliding formulations: finite-sliding, and small-sliding (Simulia 2007). Finite-sliding was specified for the cup-acetabulum contact pair because it is an appropriate formulation for surfaces that undergo arbitrary separation and motion relative to one another. Small-sliding was specified for the impactor-cup contact pair because it is appropriate for surfaces that undergo little relative motion. Both of these choices were also used in the related work by Yew et al. (2006).

Lastly, the type and magnitude of friction between the surfaces was specified for each contact pair. While real world measurements show that the relationship between tangential force and displacement is in fact nonlinear, this thesis makes a typical simplification, that the friction between contact pairs is Coulomb friction (Shirazi-Adl et al. 1993; Yew et al. 2006). The available Coulomb friction models in ABAQUS are: Frictionless, Pen-

alty (stiffness), Static-Kinetic Exponential Decay, Rough, Lagrange Multiplier, and User-defined (Simulia 2007). ABAQUS's Frictionless model was used to model "friction" between the impactor-cup contact pair, because it was used by Yew et al. (2006) and it specifies that the surfaces in contact may slide freely along one another.

The Penalty model was used to model friction between the cup and acetabulum. This model allows for some relative motion (i.e., elastic slip) between the contact surfaces when they should be sticking, in order to facilitate rapid solution convergence. Static-Kinetic Exponential Decay and User-defined friction models were not used because measurement of the required experimental parameters was beyond the scope of this thesis. The Rough friction model was not used because this model assumes that the surfaces cannot slide along one another. The Lagrange Multiplier model, although similar to the Penalty model in that it also allows for stick-slip motion, was not used because it enforces sticking more strictly and is therefore more computationally expensive and can hinder solution convergence (Simulia 2007).

The coefficient of friction between the resurfacing cup and the reamed acetabulum during the press-fitting procedure has significant implications on modeling of cup seating (Spears et al. 1999). Previous studies have specified the degree of friction between the cup and acetabulum with friction coefficient values ranging from 0.5 to 0.62 (Udofia et al. 2007; Yew et al. 2006). These values are based on a study of friction between cancellous bone of cadaveric tibiae and two different brands of titanium bead-coated metal, under various normal pressures at the interface (Shirazi-Adl et al. 1993). This range of friction values may not be valid for cortical bone, however, but the amount of cortical bone in contact with the cup is relatively small (i.e., at the rim of the acetabulum only) com-

pared to the amount of cancellous bone involved. A coefficient of friction value of 0.57 was used for the finite element models of this thesis, as it is the average of the six friction coefficients measured by Shirazi-Adl et al. (1993); and it is also a compromise between the values of 0.5 and 0.62 used by Udofia et al. (2007) and Yew et al. (2006), respectively.

3.4 Simulation of cup insertion

This section describes the methodologies used to simulate the surgical procedure of cup insertion, which involves initial placement and press-fitting of the resurfacing cup into the acetabulum. Three different methods of press-fitting were tested in the 2D axisymmetric model to determine what method would be most suitable for use in the anatomically accurate 3D model.

To simulate the surgical insertion of the cup into the acetabulum, the cup in the 3D model must first be carefully positioned before press-fitting can take place. In clinical practice, the resurfacing cup is typically positioned with 45˚ abduction, and 15-20˚ anteversion (Burnell 2007). Unfortunately, determination of this positioning is not possible with the hemi-pelvis alone, so the cup was oriented and placed in alignment with a plane fit to the acetabular rim instead. The plane was defined by selecting three points on the rim of the acetabulum (*N.B.* this is the same plane defined during the 2D axisymmetric geometry construction, as shown in Figure 8 in Section 3.1). The cup was then positioned such that it rested on the ilial and ischial bony prominences of the acetabular rim.

The direction of implantation was defined via a line normal to the plane and through the centre of the cup.

Three methods of press-fitting are simulated in this thesis: multiple-displacement, multiple-displacement variation, and multiple-load. The multiple-displacement methods simulate press-fitting via applied displacements, and the multiple-load method simulates press-fitting via applied forces. The procedures for these methods are quite similar. In each of these methods contact is first established between the cup and acetabulum, and then between the impactor and cup rim, after which the cup is pushed into the acetabulum. Contact between the cup and acetabulum is established in the first step of the analysis by specifying a nominal cup displacement into the acetabulum of 1 μm in the multiple-displacement methods, and 25 μm in the multiple-load method (a displacement smaller than 25 μm resulted in analysis abortion). During this step, the rigid impactor is fully constrained at a position of 1 μm above the cup rim to prevent rigid body motion and interference with contact establishment. Physical constraints are also applied to both the cup and pelvis in this step. In the anatomically accurate model, lateral translation constraints are specified through the pole of the cup to constrain the cup to only move in the direction of implantation and to prevent lateral translation and rotation of the cup during insertion (see Figure 14).

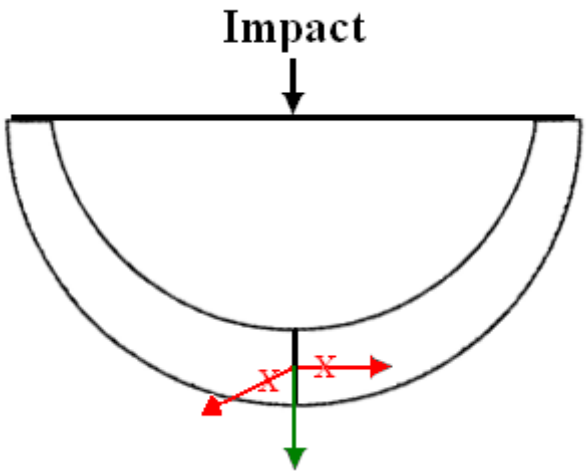

Figure 14: Cup Constraints
Constraints are applied through the pole of the cup such that lateral translations are prevented (red arrows) and only translation in the direction of implantation is allowed (green arrow).

The cup constraints are specified because surgeons normally observe no lateral translation nor rotation of the cup during the press-fitting procedure (Turgeon 2009). Constraints on the pelvis are specified in both the 2D axisymmetric and 3D models. The base of the pelvic geometry is fully constrained in the 2D axisymmetric model (i.e., all degrees of freedom of nodes and elements in the base are constrained) (Yew et al. 2006). The sacral-iliac and pubic symphysis joint regions are similarly constrained in the 3D model (Udofia et al. 2007). Figure 15 depicts the constrained region in 2D axisymmetric model, and Figure 16 depicts the constrained regions in the 3D model.

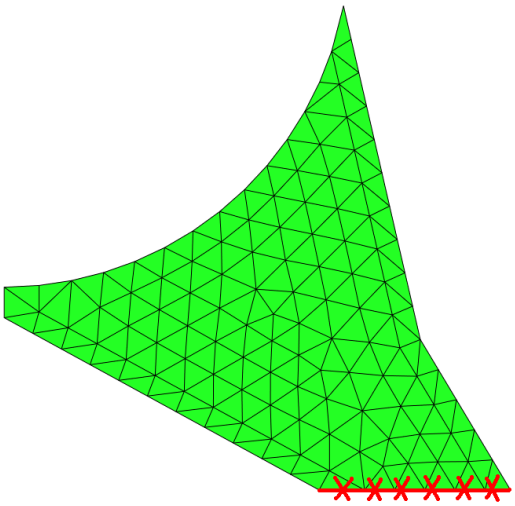

Figure 15: 2D Axisymmetric Pelvic Geometry Constraints
The base of the 2D axisymmetric pelvic geometry is fully constrained.

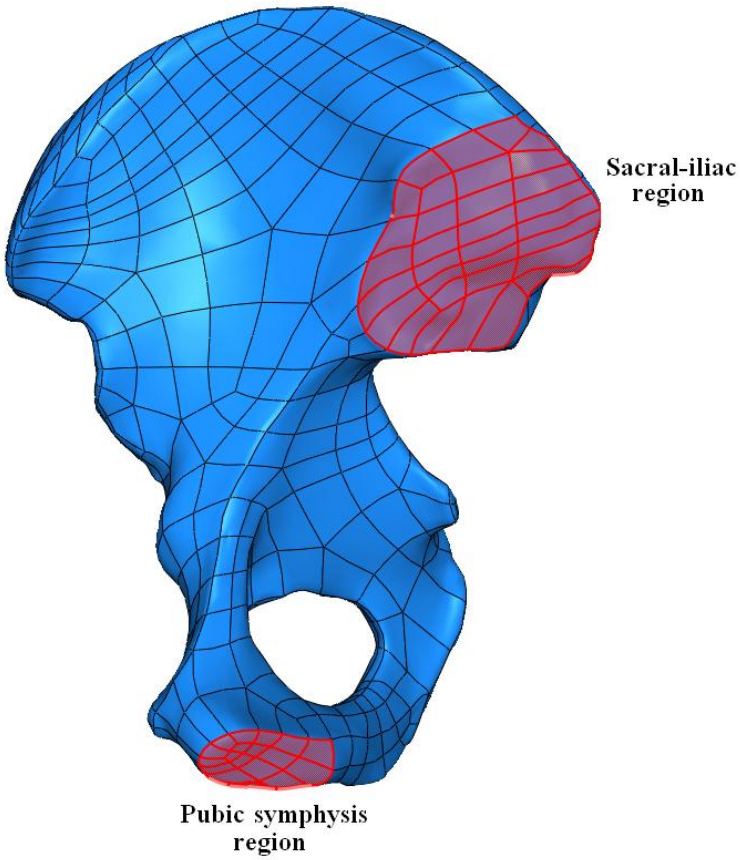

Figure 16: 3D Pelvic Geometry Constraints
The sacral-iliac and pubic symphysis joint regions are fully constrained.

After the first step establishes contact between the cup and acetabulum, contact is then established between the impactor and the rim of the cup. In the multiple-displacement methods, a displacement of 1 μm is assigned to the impactor in the direction of implantation; in the multiple-load method a displacement of 26 μm is assigned (again, a smaller displacement resulted in analysis abortion). In addition, a small negative pressure of 1000 Pa is applied to the rim of the cup to firmly establish contact by preventing the potential for recurrent opening and closing of the contact nodes (i.e., chattering) arising from poor contact establishment via the small impactor displacements (Simulia 2007). In the multiple-load method, a stabilizing load of 0.05 N is applied (Yew et al. 2006). The small displacement constraint applied to the cup in the previous step is maintained in this step.

Once contact is established between the cup and acetabulum, and between the impactor and cup, the next steps simulate press-fitting by pushing the cup into the acetabulum via prescribed displacements or applied forces. Firstly, the small cup displacement and the -1000 Pa pressure on the cup rim are deactivated, and then two steps are required per simulated impact. In the multiple-displacement methods, the impactor displacement is modified to push the cup a specific amount into the acetabulum to simulate impact. The impactor displacement is then deactivated in order to allow the displaced cup to rebound in the second step. The multiple-displacement and multiple-displacement variation methods differ only by how the cup is pushed the distance equal to the initial gap between the poles of the cup and acetabulum. The cup is pushed this distance in one impact step in the former method, and in three equivalent impact steps in the latter. After the

cup is pushed a distance equal to the initial polar gap, subsequent impacts push the cup by several additional 1 mm incremental displacements (Yew et al. 2006).

The multiple-load method follows the same procedure as that of the multiple-displacement method, but with applied forces instead of displacements. In the first impact, the existing displacement on the impactor is deactivated to allow for force application. The force applied in the first impact is the force corresponding to the applied displacement in the first impact of the multiple-displacement analysis (30.5 kN in this thesis). The force is then deactivated in the next step (and in all other rebound steps) to simulate cup rebound. Each of the subsequent impacts increases the force by a factor of 1.5 until the analysis diverges. The stabilizing load is also propagated in all steps to maintain contact between the impactor and cup rim during cup rebound.

Chapter 4

Results and Discussion

This chapter presents and discusses the results obtained from the two-dimensional axi-symmetric and anatomically accurate three-dimensional finite element analyses of press-fitting of a resurfacing cup. The 2D axisymmetric results show which of the tested press-fitting methods is the most appropriate for use with an anatomically accurate model. The 3D anatomically accurate results show the elastic and plastic deformation of a press-fit resurfacing cup.

4.1 2D axisymmetric analyses

One of the objectives of this thesis was to determine the most appropriate press-fitting method to use in a 3D finite element model of hip resurfacing cup deformation. This was motivated by unresolved issues pertaining to the comparison of two press-fitting methods – namely multiple-displacement (MD) and multiple-load (ML) – in a previous finite element study conducted by Yew et al. (2006). In this thesis, a series of 2D axisymmetric analyses were run to assess different press-fitting methods. Several analyses were run for

each of the three 2D axisymmetric models in order to determine which of three tested press-fitting methods – multiple-displacement (MD), multiple-displacement variation (MDV), and multiple-load (ML) – is most suitable for use in the anatomically accurate 3D model. The first analysis of each model was used to establish when cup seating within the acetabulum was achieved during the simulation of multiple impact-rebound cycles. Impactor force versus displacement curves were then generated for each model. Convergence test results were analyzed to determine the point of convergence, and various results were compared between the models.

The aim of the first series of analyses in this thesis was to compare the impact forces between the MD method, and a variant of this method – the multiple-displacement variation (MDV) method. The MDV method was investigated because Yew et al. (2006) observed an unrealistically high impact force (100 kN) in their MD 2D axisymmetric model, and suggested that incremental displacements may reduce impact force. Cup to acetabulum contact during the press-fitting simulation was examined in order to determine when cup seating was achieved. The extent of contact between the cup and acetabulum at the end of each rebound step was determined by generating contour plots of gap distance (denoted as COPEN or contact opening in the following figures) within the limit of bony ingrowth, which in this case was chosen to be 350 μm (Yew et al. 2006), as demonstrated in Figure 17.

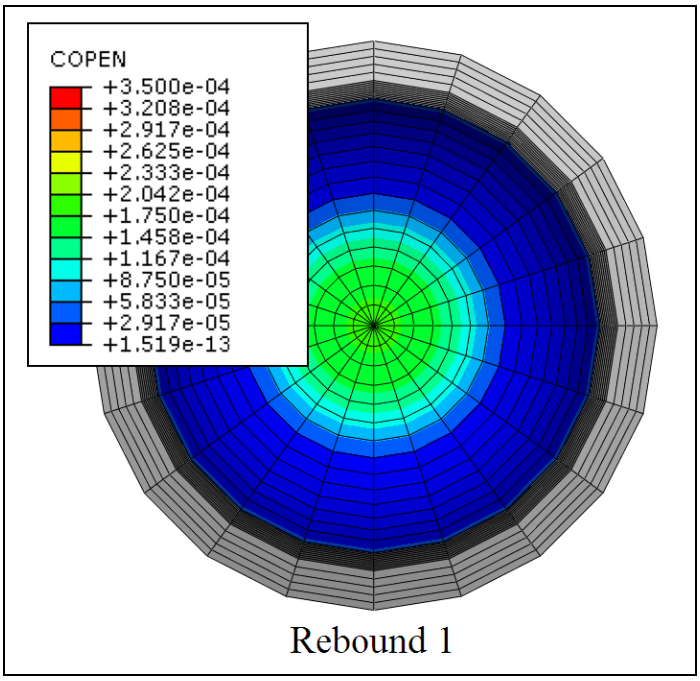

Rebound 1

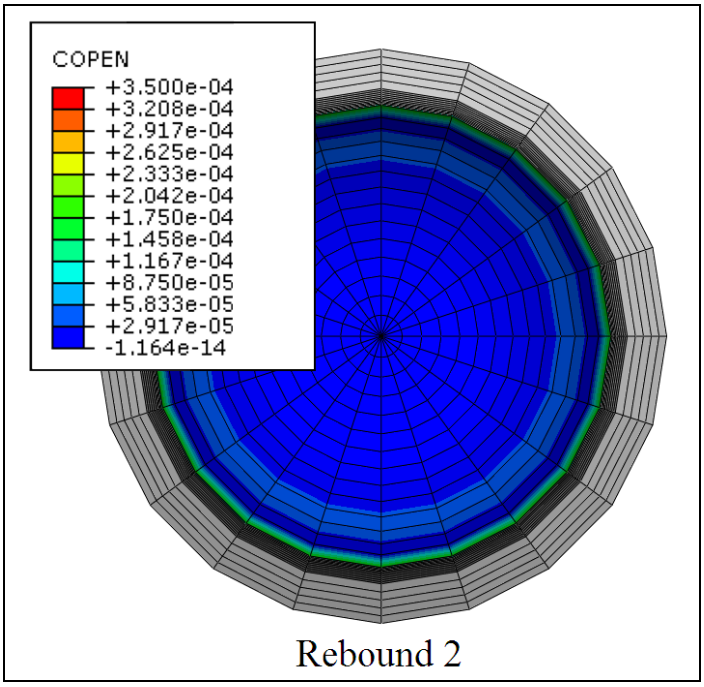

Rebound 2

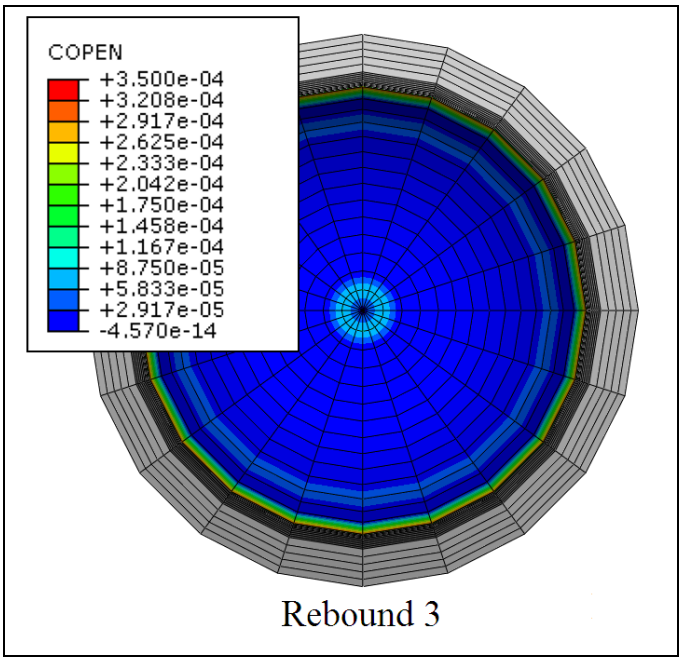

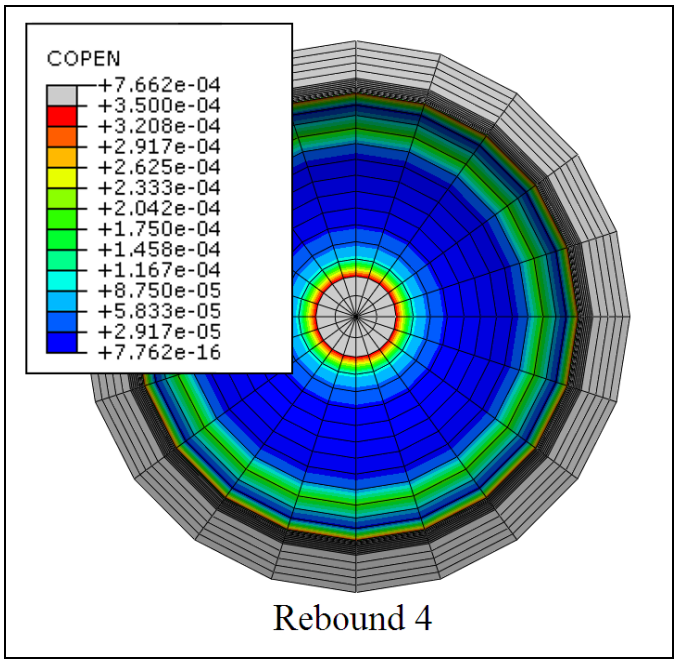

Figure 17: MD Model Cup-Acetabulum Contact Gap
Gap remaining between the cup and the acetabulum at the end of each rebound step in the MD (multiple-displacement) model (COPEN = Contact Opening). Red indicates areas having gaps at the bony ingrowth limit of 350 microns; blue indicates areas where no gaps are present (this includes areas with negative gaps resulting from over-closed surfaces). The grey area in rebound 4 indicates gaps greater than 350 microns. Units in metres.

The plots show that the gap between cup and acetabulum was less than 350 μm – and therefore the cup could be considered seated – at the end of rebounds 1, 2, and 3. At the pole of the acetabulum, the gap was smallest at the end of rebound 2, and then got larger in rebounds 3 and 4. Therefore, the best seating appears to have been achieved at the end of rebound 2. The gap thereafter increased due to deformation of the floor of the acetabulum, as shown in Figure 18. Nearly identical cup seating results were exhibited by the MDV model.

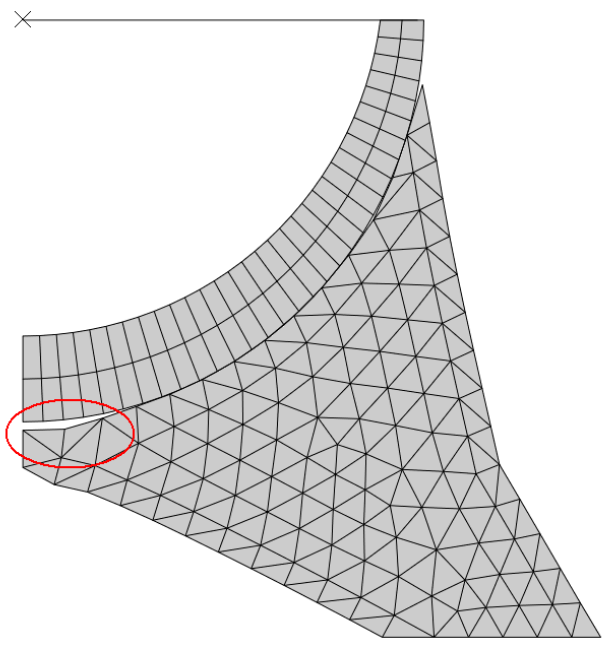

Figure 18: MD Model Acetabular Floor Deformation
Deformation at the end of rebound 4 in the MD model circled in red.

Von Mises stress distributions in the cortical and cancellous bone regions were examined to further assess cup seating according to the Von Mises criterion (Doblaré et al. 2004). It must be noted that these stresses were overestimated because the plastic strain

values used as bone material inputs were miscalculated. The plastic strain values were underestimated by 3% in the cortical bone, and 16% in the cancellous bone. We believe the complexities of the models are well represented despite this error, and that the modalities of deformation seen are likely to appear in a real system. Contour plots of the stress values lying between the assumed yield and ultimate strength limits for each bone type at the end of impacts 1 and 2 were generated. Bone fracture was assumed in regions where the von Mises stress reached the ultimate strength limit, as depicted in Figure 19.

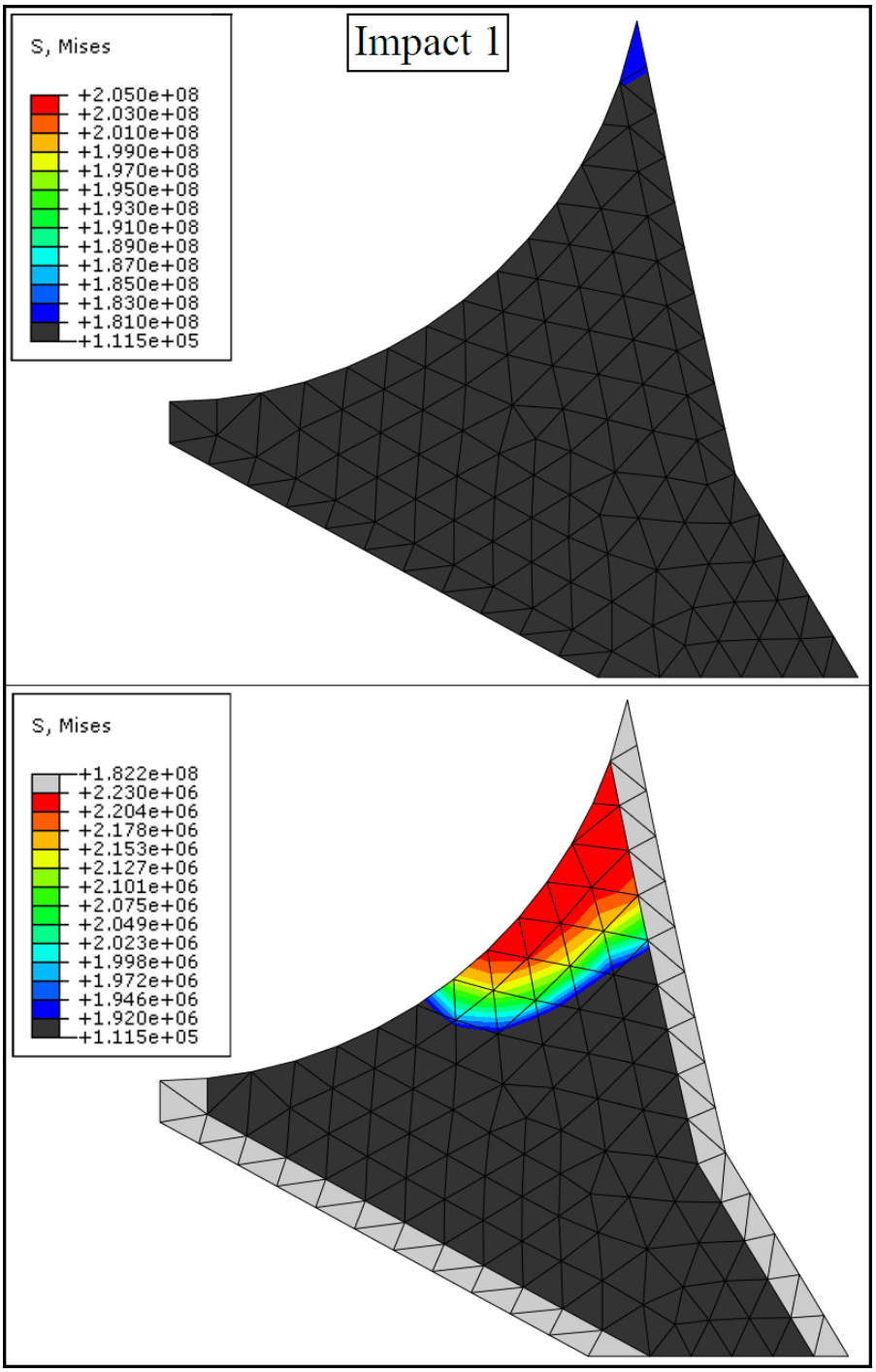
Impact 1
S, Mises
+2.050e+08
+2.030e+08
+2.010e+08
+1.990e+08
+1.970e+08
+1.950e+08
+1.930e+08
+1.910e+08
+1.890e+08
+1.870e+08
+1.850e+08
+1.830e+08
+1.810e+08
+1.115e+05
S, Mises
+1.822e+08
+2.230e+06
+2.204e+06
+2.178e+06
+2.153e+06
+2.127e+06
+2.101e+06
+2.075e+06
+2.049e+06
+2.023e+06
+1.998e+06
+1.972e+06
+1.946e+06
+1.920e+06
+1.115e+05

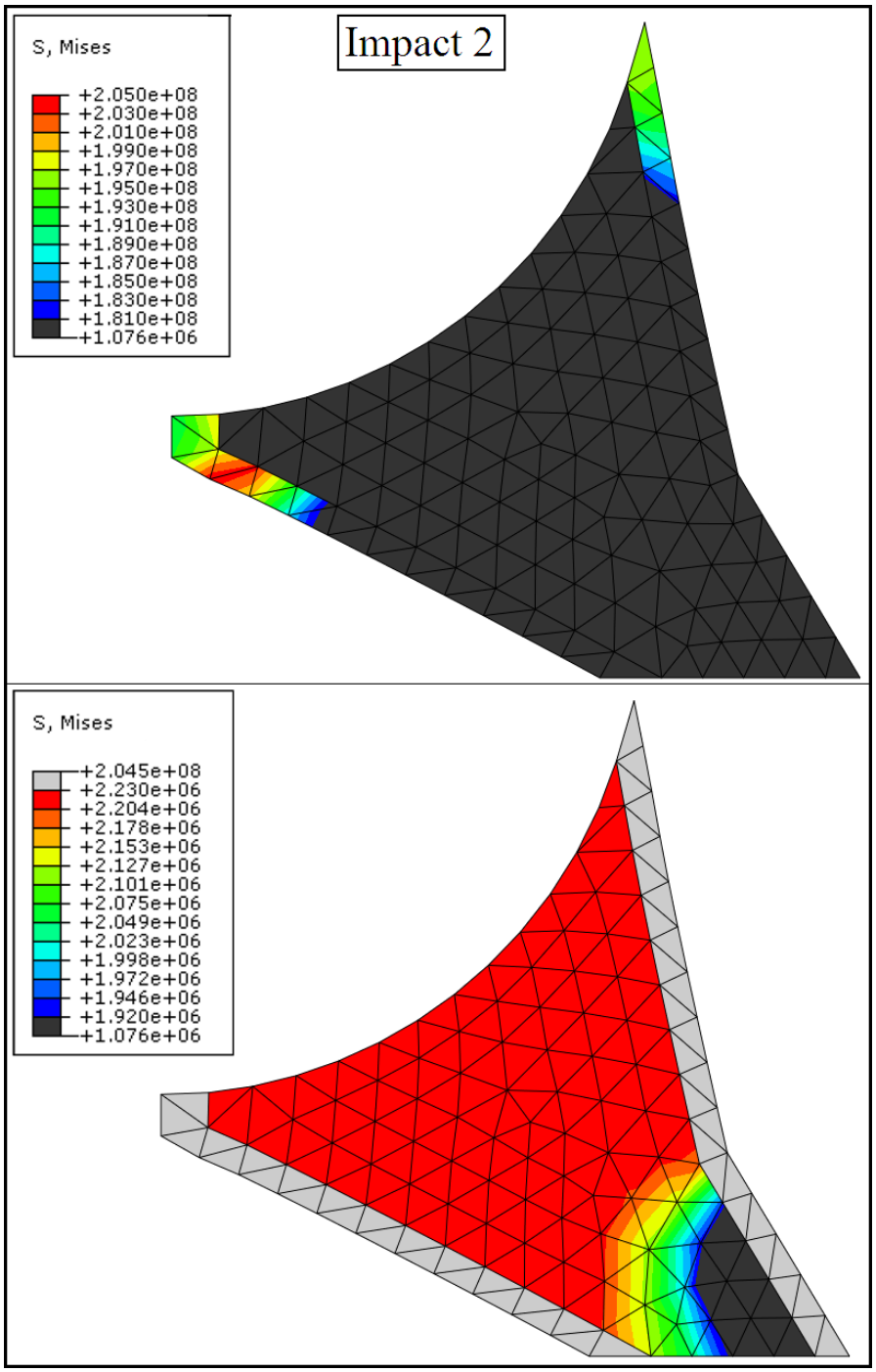

Figure 19: MD Model Von Mises Stresses
Von Mises stresses in the cortical and cancellous bone regions (top and bottom panels for each impact, respectively) at the height of impacts 1 and 2 in the MD model. Blue indicates areas where the von Mises stress has reached the yield stress (i.e., where bone has deformed plastically); red indicates areas where the von Mises stress has reached the ultimate strength (i.e., where bone has fractured). Units in pascals.

The von Mises stress plots for both the MD and MDV models show that some plastic deformation and fracture occurred towards the rim of the acetabulum in the cortical and cancellous bone regions, respectively, during the first impact. These stress distributions occurred because the cross-section through the acetabulum near the rim is relatively thin compared to the rest of the pelvic geometry. In the second impact, bone yield and fracture occurred throughout most of the cancellous bone region, and in the cortical bone at the floor of the acetabulum in addition to at the acetabular rim. These stress distributions occurred because the cup was pushed beyond the initial polar gap distance by 1 mm, pushing the floor of the acetabulum down and therefore causing excessive deformation. Therefore, cup seating was considered to have been achieved after the first impact (rebound 1) instead of the second impact, in order to preserve the structural integrity of the acetabulum. This is in contrast to the studies of Yew et al. (2006) and Spears et al. (1999), wherein multiple impacts were used to seat the cup. These studies did not include yield behaviour in bone, but assumed only linear elasticity. This thesis has shown that such an assumption results in press-fitting simulations that give the illusion of realistic press-fitting in that multiple impacts are used, when in fact only one impact may be appropriate. Unfortunately, a single impact does not match with a realistic press-fitting scenario wherein multiple-impacts are used, but such is the nature of a static-based (as opposed to a dynamic-based) simulation.

With rebound 1 established as the step in which cup seating was achieved in both the MD and MDV models, impactor force was plotted against cup displacement during impact for all seven analyses in each model, as shown in Figures 20 and 21.

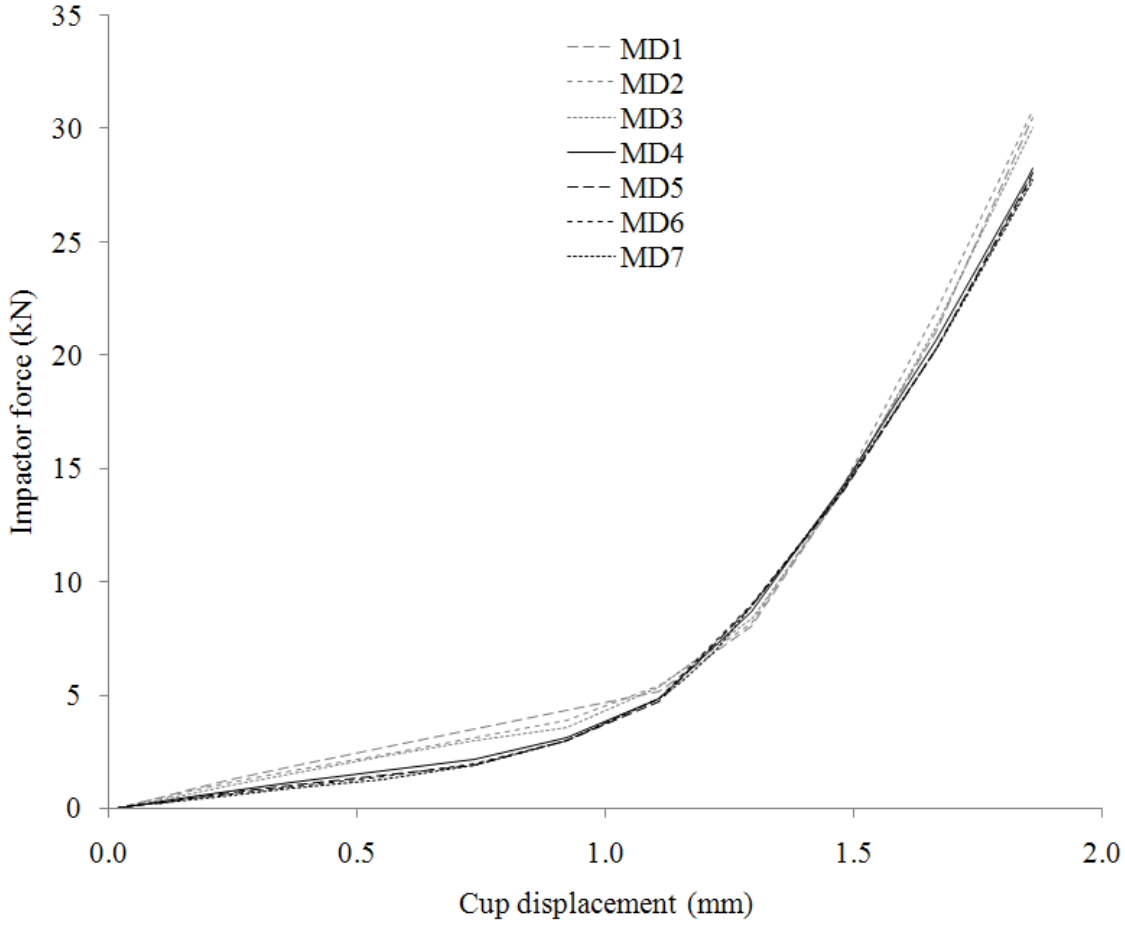

Figure 20: MD Model Impactor Force Versus Cup Displacement
Force versus displacement curves are shown for all seven analyses. Cup displacement was measured with respect to the inner pole of the cup.

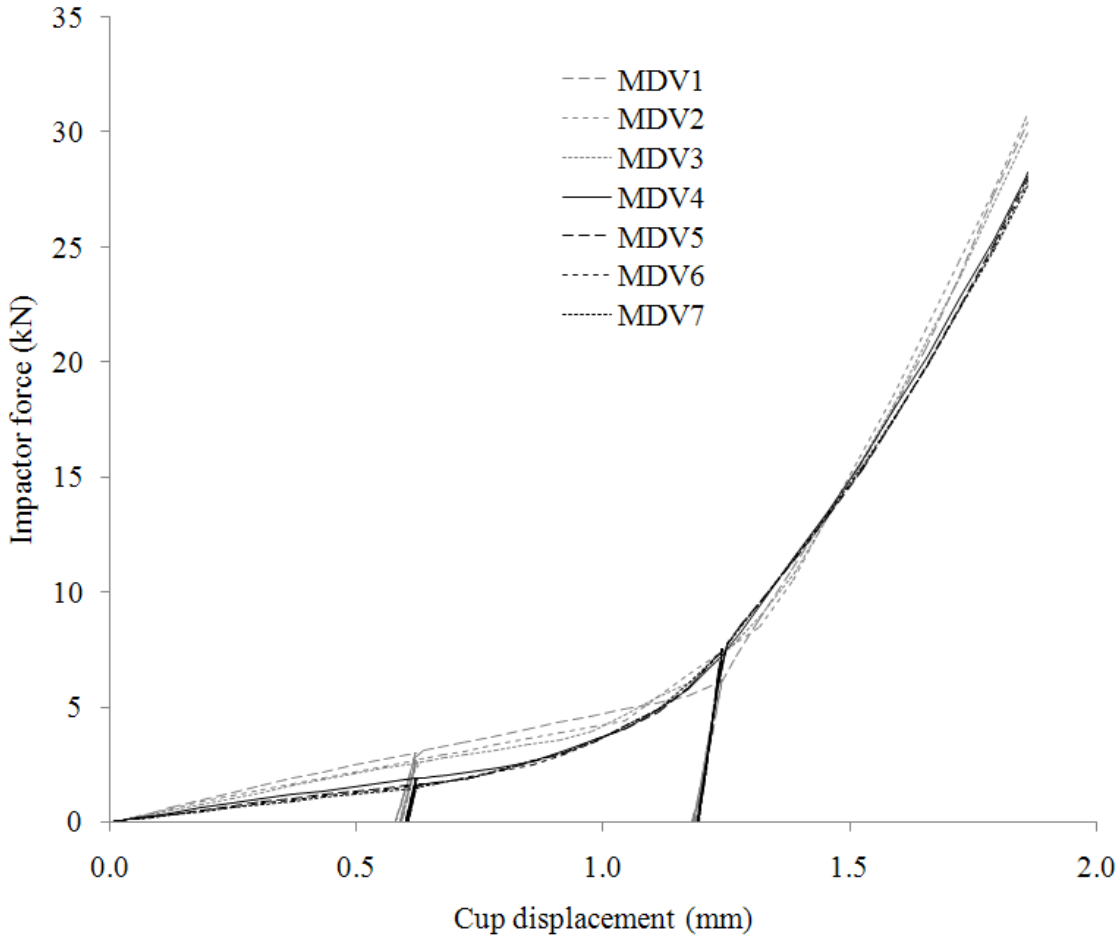

Figure 21: MDV Model Impactor Force Versus Cup Displacement
Force versus displacement curves are shown for all seven analyses. Cup displacement was measured with respect to the inner pole of the cup.

The MD and MDV force versus cup displacement curves differ very little. The MDV curves are different in that they include the displacements corresponding to the two re-bound steps prior to a displacement equivalent to the initial polar gap distance (1.86 mm). In both models, the force required to displace the cup through the 1.86 mm decreases as the mesh density increases, and appears to converge at approximately 28 kN. Table 5 compares the impact force corresponding to the polar gap displacement for each analysis of the MD and MDV models.

Table 5: Impactor Force Comparison Between the MD and MDV Models
The impactor force at the height of impact (i.e., the point at which the cup has displaced the initial polar gap distance, 1.86 mm) for each analysis. The percent differences between these forces are also shown.

Analysis No.	Force (kN)		% |Δ|
	MD	MDV	
1	30.48	30.44	0.13
2	30.68	30.67	0.03
3	30.03	30.01	0.07
4	28.25	28.23	0.07
5	28.10	28.08	0.07
6	27.92	27.91	0.04
7	27.72	27.72	0

Total internal energies (ABAQUS output variable: ALLIE) were analyzed to determine when convergence occurred. Convergence was achieved in the fourth analysis of each of the MD and MDV models, as the corresponding change in total internal energy was within two percent of the two previous analyses, as shown in Tables 6 and 7.

Table 6: Total Internal Energies of the MD Analyses
Total internal energy (i.e., total strain energy) at the end of rebound 1 for each analysis in the MD model. The greatest absolute difference in total internal energy relative to the third analysis in each set of three successive analyses is shown.

Analysis No.	Total Internal Energy (J)	$\% \lvert\Delta\rvert_{Max}$
1	3.103	–
2	3.195	–
3	3.204	3.3
4	3.183	0.7

Table 7: Total Internal Energies of the MDV Analyses
Total internal energy at the end of rebound 1 for each analysis in the MDV model. The greatest absolute difference in total internal energy relative to the third analysis in each set of three successive analyses is shown.

Analysis No.	Total Internal Energy (J)	% $\|\Delta\|_{Max}$
1	3.149	–
2	3.231	–
3	3.236	2.8
4	3.219	0.5

Analysis 4 in each of the MD and MDV models was used to compare results of interest. As already seen in Figures 20 and 21, and in Table 5, the impactor forces were very similar between the two models; the maximum force on the impactor during the impact that achieved cup displacement equivalent to the initial polar gap in the each of the MD and MDV models was nearly the same (28.25 and 28.23 kN, respectively). These models yielded other nearly identical results as well. The polar gap remaining after cup seating differed only by 1 micron (161 and 160 μm, respectively). The energy outputs at the end of rebound were similar, with the exception of frictional dissipation (and therefore total energy), as shown in Table 8.

Table 8: MD and MDV Model Energy Outputs
To add up the energies, the following equations apply:
Residual energy = Total internal energy + Frictional dissipation – External work;
Total internal energy = Strain + Artificial strain + Plastic dissipation energies.

Energy Quantity	MD	MDV	|Δ|	% |Δ|
Residual (J):	1.316	0.472	0.844	64.13
Total Internal:	3.183	3.219	0.036	1.13
Strain	2.238	2.242	0.004	0.18
Artificial Strain	0.001	0.001	0	0
Plastic Dissipation	0.944	0.976	0.032	3.39
Frictional Dissipation	9.221	8.3	0.921	9.99
External Work	11.088	11.065	0.023	0.21

Radial cup deformations based on a spherical coordinate system located at the centre of the cup in the cup rim plane were also quite similar, as shown in the contour plots of Figure 22.

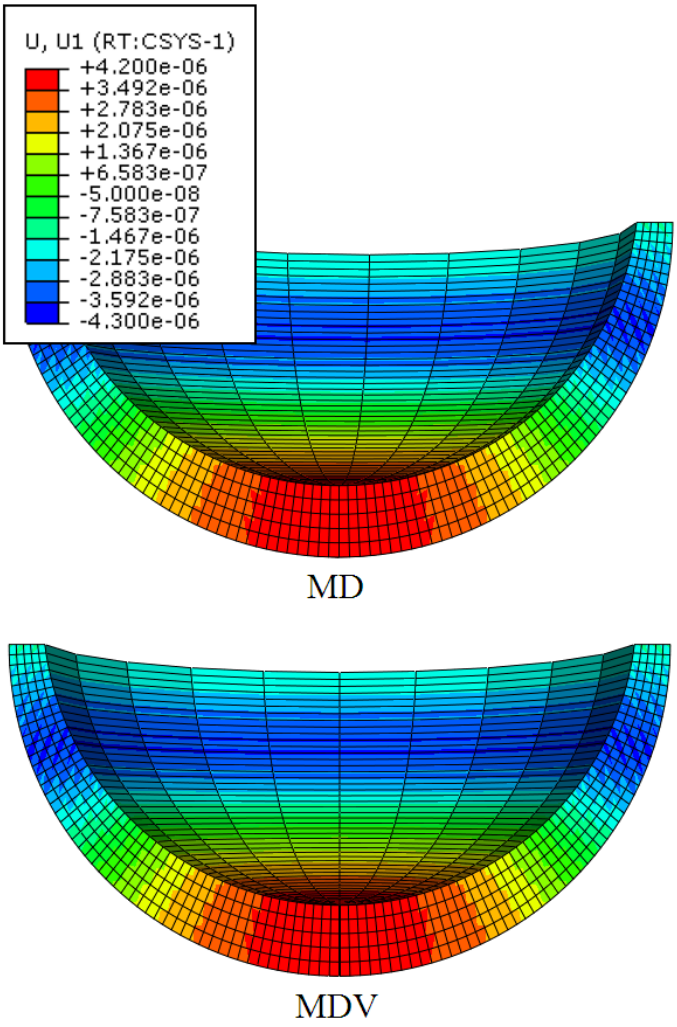

Figure 22: MD and MDV Model Radial Cup Deformation
Radial cup deformation at the end of rebound, as determined via a spherical coordinate system located at the centre of the cup in the cup rim plane. Red (+) denotes expansion, blue (-) compression. Units in metres.

Figure 22 shows the occurrence of maximum radial cup deformation (4.3 µm of compression) below the cup rim near the rim of the acetabulum (the cup was sitting proud). The bearing clearance is smaller at this point and is more likely to be compromised thereat than at the rim of the cup. This is a clear example of how measurement of cup deformation via diametral deformation at the rim is insufficient; diametral deformation at

the rim of the cup provides useful indications of cup deformation only if maximum cup deformation occurs at the rim of the cup.

The use of incremented displacements instead of a single displacement to push the cup a distance equivalent to the initial polar gap in the MDV model did not reduce the impact force required. Therefore, the MDV method of press-fitting was not pursued in favour of either the MD or ML method. The aim of the next series of analyses in this thesis was to compare the MD and ML methods. This was motivated by the statement of Yew et al. (2006) that the ML method was more realistic than the MD method because of the high impact force seen in the latter. This statement is confusing, because the initial impact force input in the ML model was obtained from the output of the MD model. Cup seating in the ML model occurred at the end of impact 1, because of excessive stresses in the bone indicative of fracture during the second impact. To assess the equivalency of the MD and ML models, force versus displacement curves during impact were generated for the ML analyses, and they show close agreement with the MD curves (see Figure 23 and Table 9).

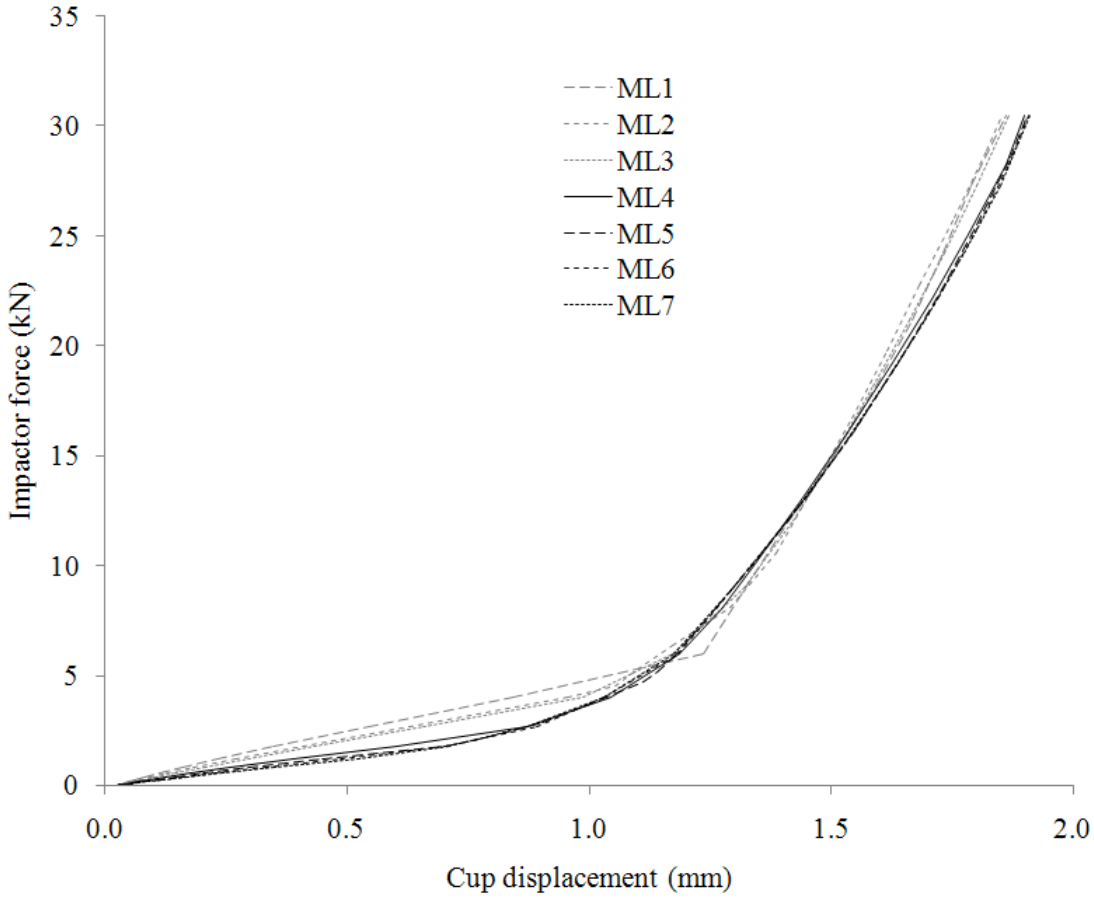

Figure 23: ML Model Impactor Force Versus Cup Displacement
Force versus displacement curves are shown for all seven analyses. Cup displacement was measured with respect to the inner pole of the cup.

Table 9: Impactor Force Comparison Between the MD and ML Models
The impactor force at the height of impact (i.e., the point at which the cup has displaced the initial polar gap distance, 1.86 mm) for each analysis. The percent differences between these forces are also shown.

Analysis No.	Force (kN)		% |Δ|
	MD	ML	
1	30.48	30.48	0
2	30.68	30.48	0.65
3	30.03	30.11	0.27
4	28.25	28.25	0
5	28.10	28.09	0.04
6	27.92	27.91	0.04
7	27.72	27.77	0.18

Convergence testing was performed to determine which of the ML and MD methods was more computationally efficient. This was done because Yew et al. (2006) chose to use the MD method based on faster runtimes, but they did not perform convergence testing. The convergence testing for comparison of the ML and MD methods showed that the ML model did not converge (see Table 10). Therefore, of the three press-fitting methods tested in this thesis, the MD method was deemed to be the most appropriate for use in the anatomically accurate model.

Table 10: Total Internal Energies of the ML Analyses
Total internal energy at the end of rebound 1 for each analysis in the ML model. The greatest absolute difference in total internal energy relative to the third analysis in each set of three successive analyses is shown.

Analysis No.	Total Internal Energy (J)	% $\lvert\Delta\rvert_{Max}$
1	3.156	–
2	3.202	–
3	3.314	5.0
4	3.590	12.1
5	3.609	8.9
6	3.664	2.1
7	3.712	2.9

Various results from the ML analyses were compared to those of the MD analyses to investigate the reason for lack of convergence. One key difference between the ML and MD models is that as the mesh density increased, the maximum force on the impactor decreased in the MD model compared to the preset constant value in the ML model (Figure 24).

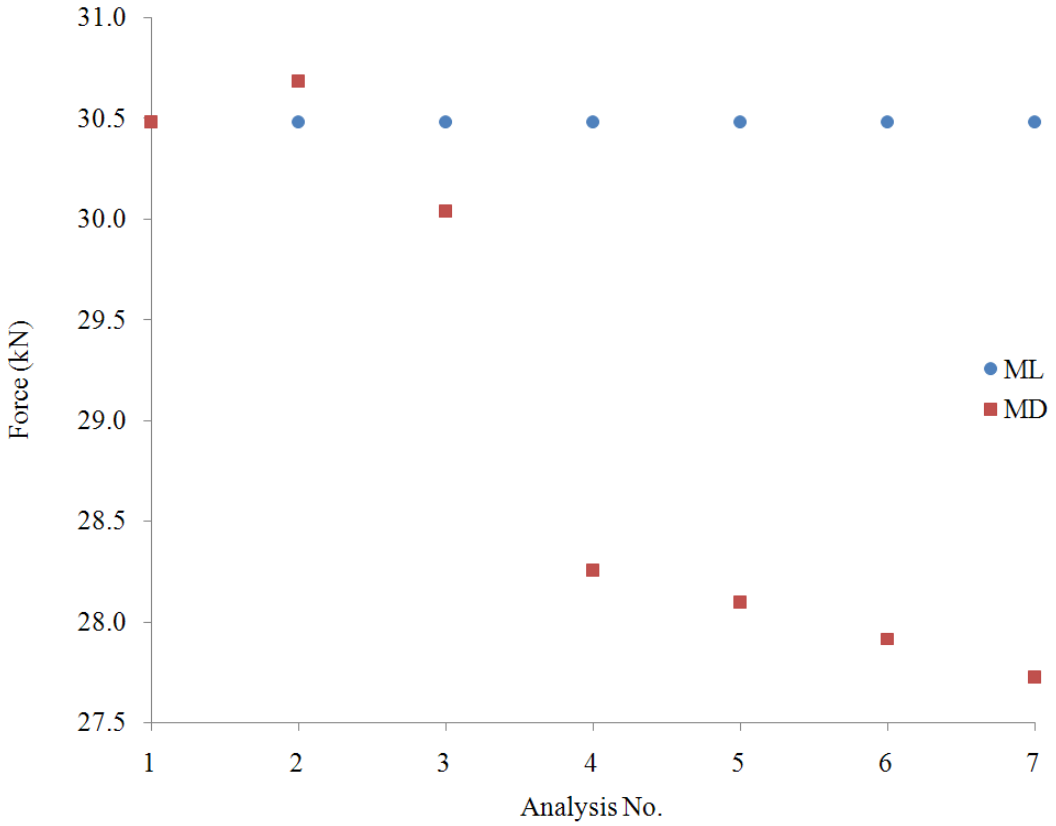

Figure 24: Peak Impact Forces in the MD and ML Analyses

The force required to push the cup a distance equivalent to the initial polar gap (1.86 mm) decreased with increasing mesh density most likely because the smoother meshes were less stiff and therefore less resistant to cup insertion. Since the force remained constant in the ML model as the mesh density increased, the cup was pushed into the acetabulum beyond the initial polar gap distance, as shown in Figure 25.

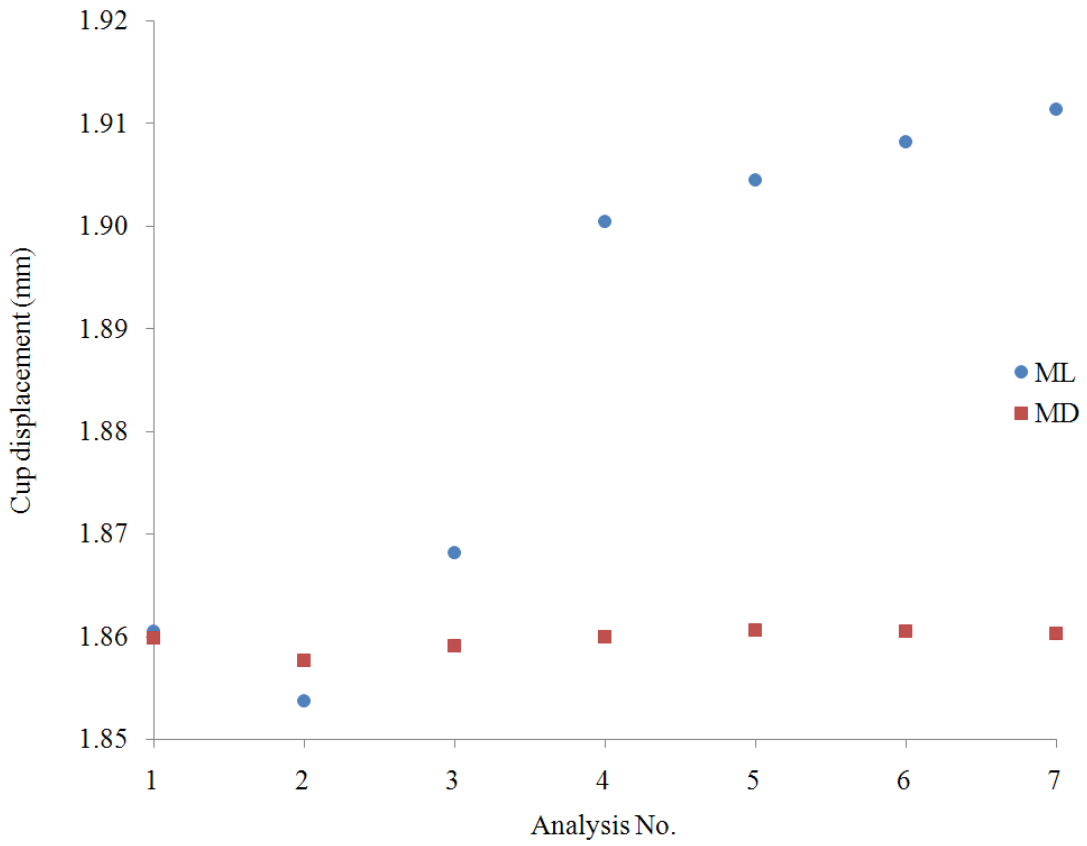

Figure 25: Cup Displacements in the MD and ML Analyses

As the cup displacement increased with increasing mesh density, the polar gap decreased and then abruptly became negative (i.e., overclosure between the polar surfaces of the cup and acetabulum occurred) in analysis 4, as shown in Figures 26 and 27.

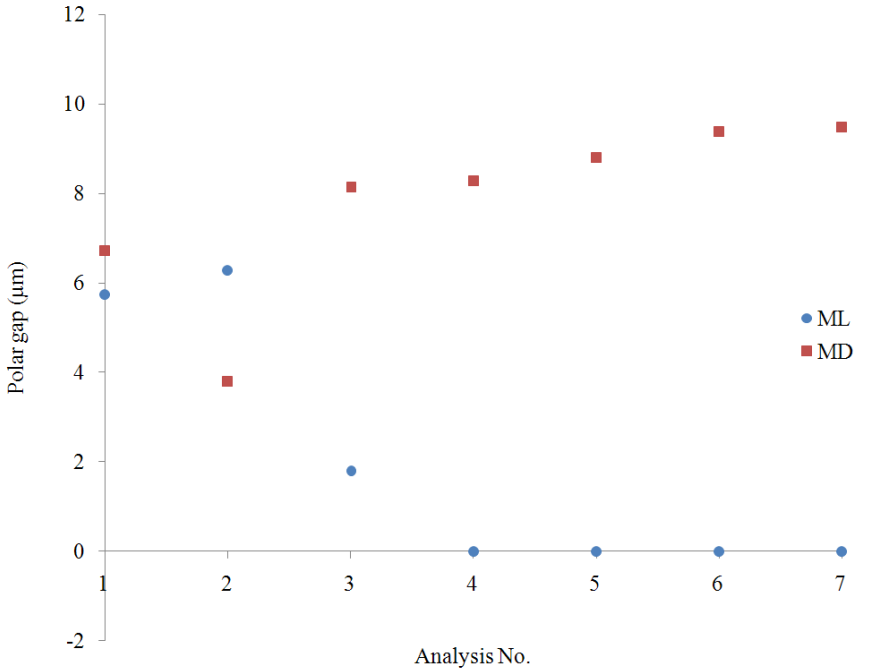

Figure 26: Polar Gaps in the MD and ML Analyses

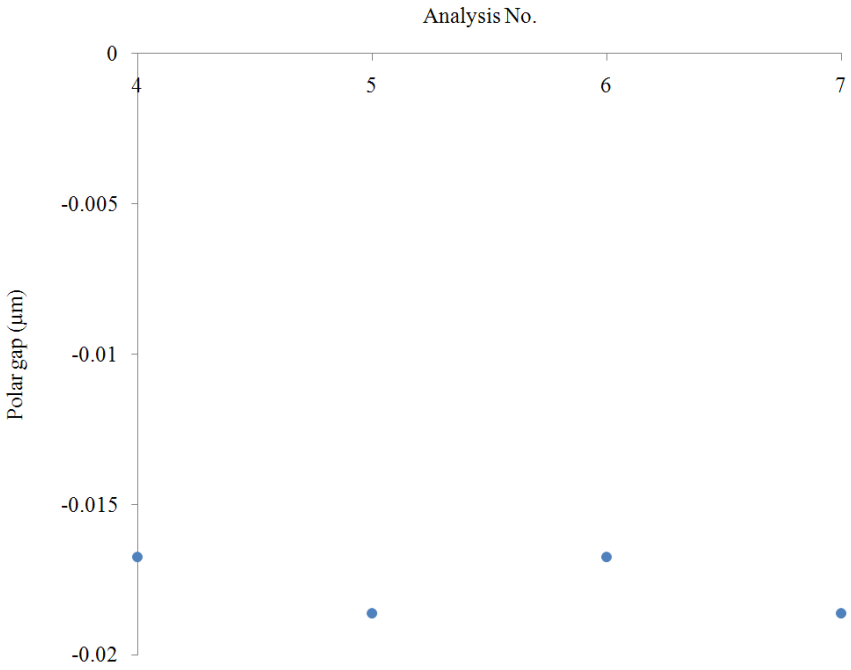

Figure 27: Negative Polar Gaps in the ML Analyses

Further assessment of the equivalency of the MD and ML models was made using analysis 1, as the forces and displacements between the two models were equivalent therein. The results of the ML model were very similar to those of the MD model; the only notable difference was in frictional dissipation, as was noted between the MD and MDV models. Table 11 shows the energies after cup rebound and Figure 28 shows frictional dissipation versus cup displacement for both impact and rebound.

Table 11: MD and ML Model Energy Outputs
To add up the energies, the following equations apply:
Residual energy = Total internal energy + Frictional dissipation – External work;
Total internal energy = Strain + Artificial strain + Plastic dissipation energies.

Energy Quantity	MD	ML	|Δ|	% |Δ|
Residual (J):	1.473	1.105	0.368	24.98
Total Internal:	3.103	3.156	0.053	1.71
Strain	2.466	2.469	0.003	0.12
Artificial Strain	0.004	0.004	0	0
Plastic Dissipation	0.633	0.683	0.05	7.90
Frictional Dissipation	10.093	9.691	0.402	3.98
External Work	11.723	11.742	0.019	0.16

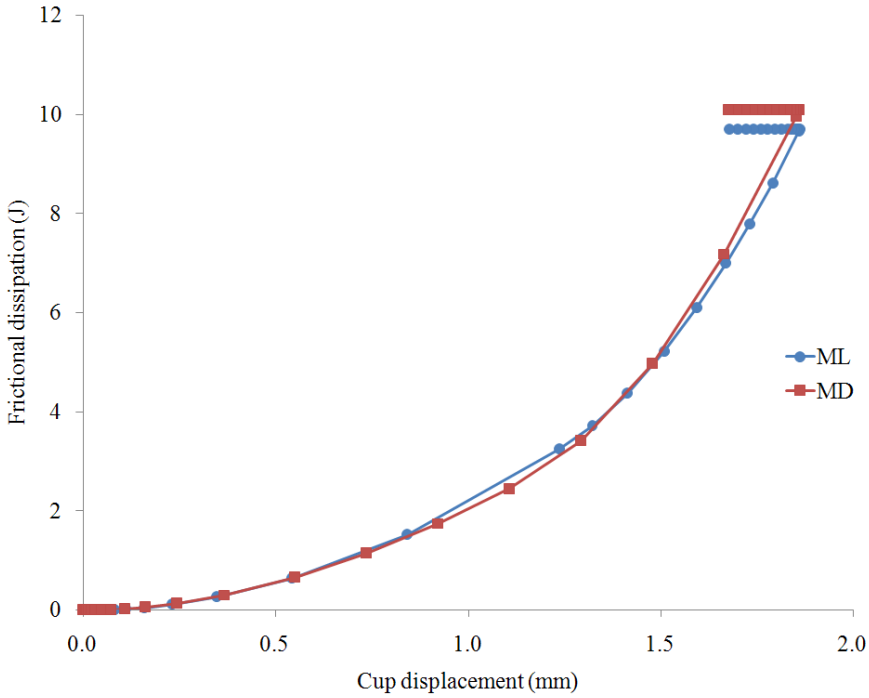

Figure 28: MD and ML Model Frictional Dissipation Versus Cup Displacement

This thesis shows that the two methods are nearly identical, again differing only in frictional dissipation energy. Therefore, the statement of Yew et al. (2006) that the ML method is more realistic than the MD method is not supported by the results of this thesis. The ML method may be perceived as more realistic in that forces are used instead of displacements to push the cup into the acetabulum. Nevertheless, a recommendation of this thesis is that the ML method not be used because contact overclosure occurs at the cup pole with mesh refinement, which is not representative of reality.

Yew et al. (2006) considered the 100 kN force they observed in their model to be unrealistic because Spears et al. (1999) used a substantially lower impact force (4 kN) to achieve cup seating in their finite element simulations of press-fitting. Yew et al. (2006)

assumed that the models of Spears et al. (1999) were somehow more correct than theirs presumably because the force used by Spears et al. (1999) was supposedly consistent with forces used in a previous experimental press-fitting study. Aside from suggesting that the large initial displacement in the MD method may have been a contributor to the high impact force, Yew et al. (2006) also pointed out differences in friction coefficients as a possible contributor. This is a reasonable assumption, since Spears et al. (1999) noted that varying the friction coefficient had a significant effect on cup seating in their press-fitting simulations. Another potentially significant contributor to the force discrepancy was the differences in material properties, but unfortunately Yew et al. (2006) did not comment on this. Yew et al.'s (2006) model consisted of arguably more realistic bone material properties that were much higher in stiffness compared to those used in the models of Spears et al. (1999). The higher stiffness would pose more resistance to cup insertion, which might explain why the impact force was much higher in the model of Yew et al. (2006) The models in this thesis used material properties more similar to those used by Yew et al. (2006), but the cancellous bone was substantially less stiff. Also, yield behaviour was specified, and as a result, larger deformations occurred. Not surprisingly, the initial impact force in the MD model of this thesis (28 kN) was lower than that of Yew et al. (2006) (100 kN). Table 12 summarizes the material properties that were used in the models.

Table 12: Summary of Cup and Bone Young's Modulus Values

Models	Young's Modulus (GPa)		
	Cup	Cortical bone	Cancellous bone
This thesis	200 (CoCr)	17	0.3
Yew et al. (2006)	210 (CoCr)	17	0.8
Spears et al. (1999)	110 (Titanium)	5.6	0.1

4.2 Anatomically accurate analyses

The anatomically accurate 3D model was used to investigate deformation of a press-fit resurfacing cup. As in the 2D axisymmetric models, determination of cup seating and convergence testing were first performed. The elastic and plastic cup deformation were then determined.

To determine when the cup was seated within the acetablum, contour plots of cup-acetabulum contact and von Mises stress distributions in the cortical and cancellous bone were generated. These plots and are shown in Figures 29 and 30.

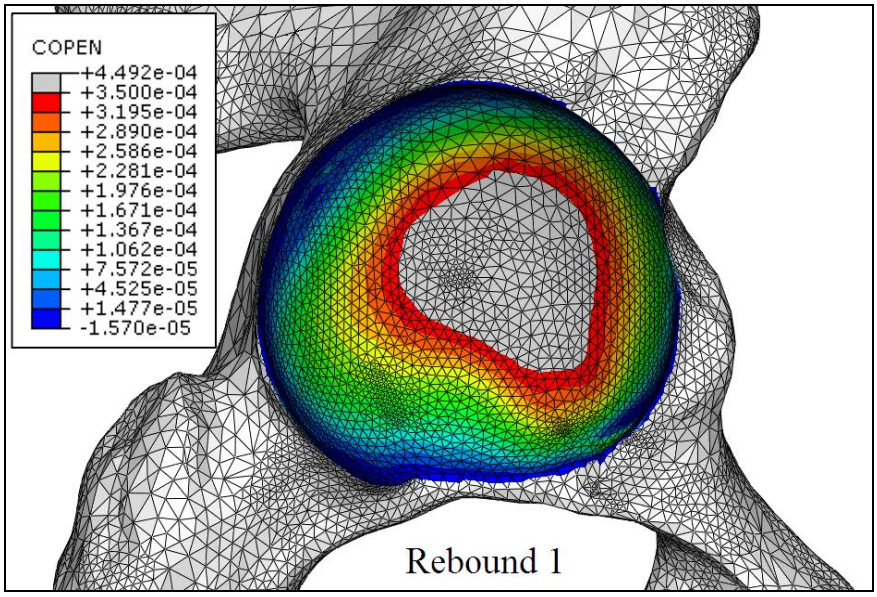

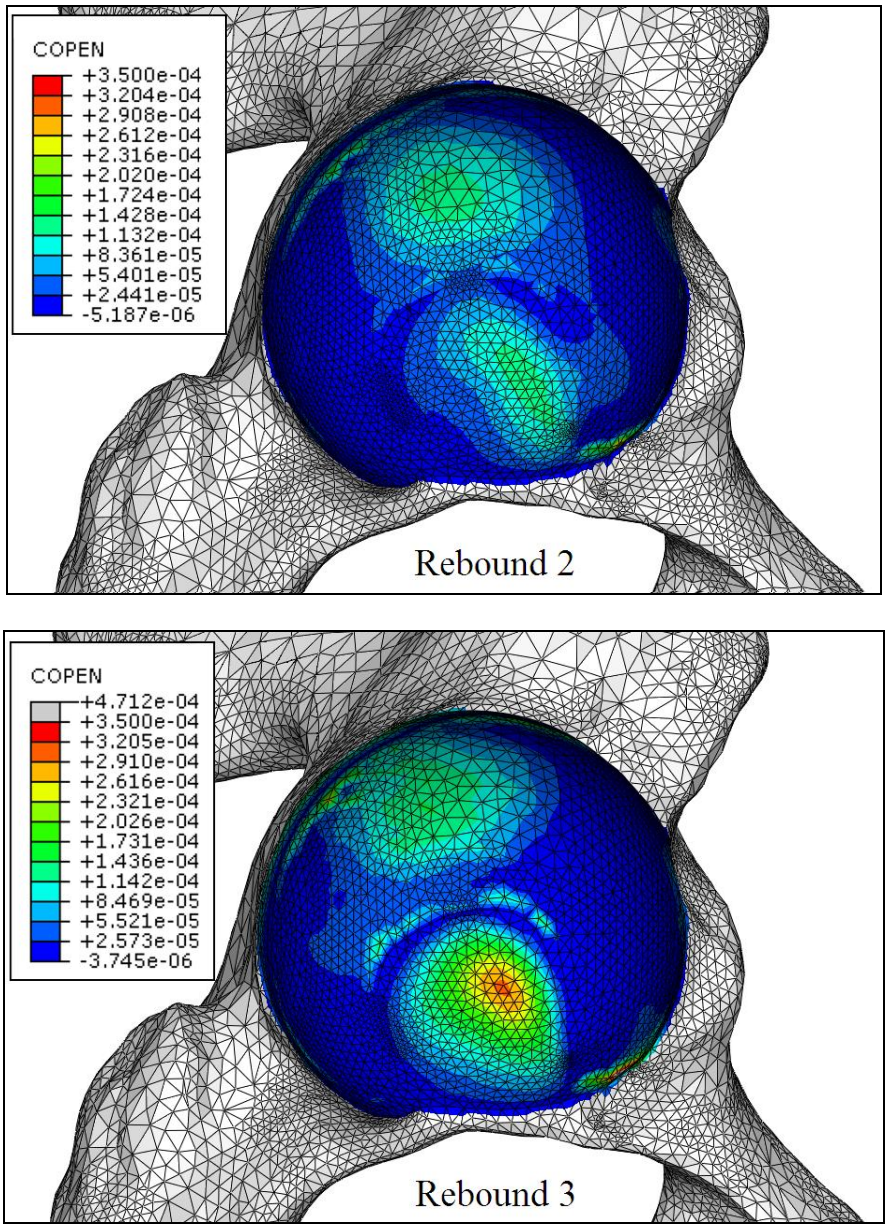

Figure 29: 3D Model Cup-Acetabulum Contact Gap
Contour plots of the gap remaining between the cup and acetabulum at the end of each rebound step in the anatomically accurate 3D model (COPEN = Contact Opening). Red indicates areas having gaps at the bony ingrowth limit of 350 microns; blue indicates areas where no gaps are present (this includes areas with negative gaps resulting from over-closed surfaces). Units in metres.

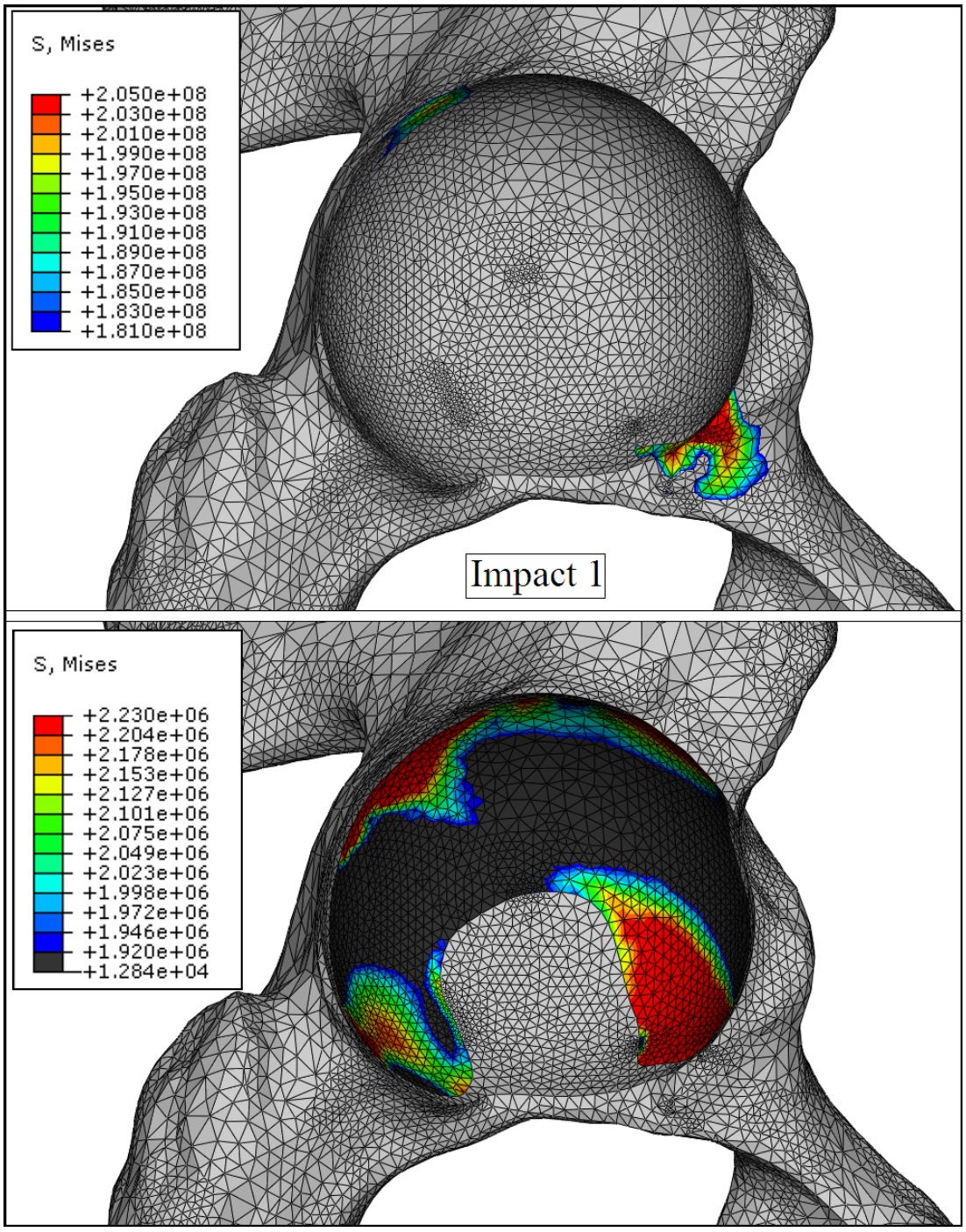
S, Mises
+2.050e+08
+2.030e+08
+2.010e+08
+1.990e+08
+1.970e+08
+1.950e+08
+1.930e+08
+1.910e+08
+1.890e+08
+1.870e+08
+1.850e+08
+1.830e+08
+1.810e+08
Impact 1
S, Mises
+2.230e+06
+2.204e+06
+2.178e+06
+2.153e+06
+2.127e+06
+2.101e+06
+2.075e+06
+2.049e+06
+2.023e+06
+1.998e+06
+1.972e+06
+1.946e+06
+1.920e+06
+1.284e+04

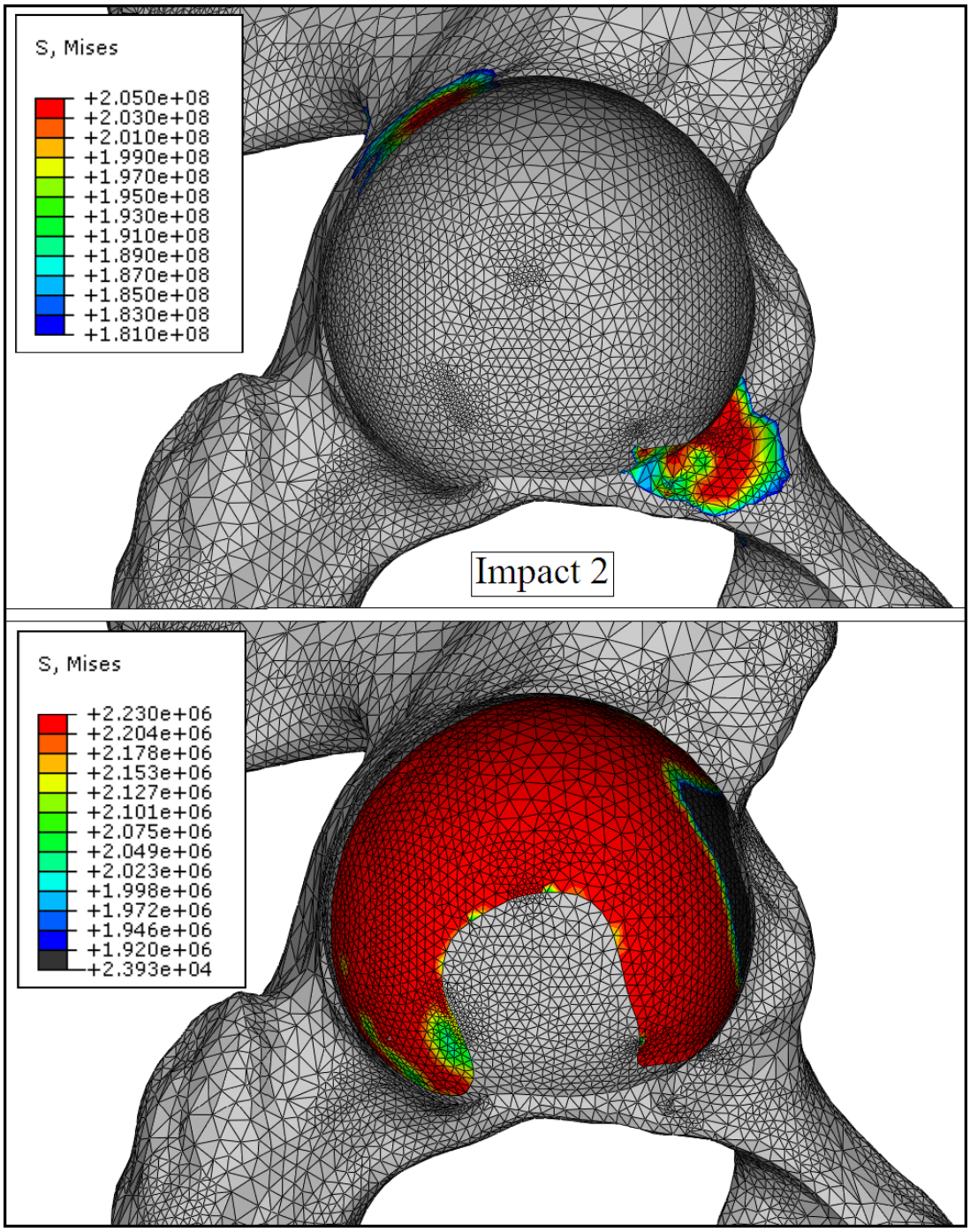

Figure 30: 3D Model Bone Von Mises Stresses
Contour Plots of von Mises stresses in the cortical and cancellous bone regions (top and bottom panels for each impact, respectively) at the height of impacts 1 and 2. Blue indicates areas where the von Mises stress has reached the yield stress (i.e., where bone has deformed plastically); red indicates areas where the von Mises stress has reached the ultimate stress (i.e., where bone has fractured).

Based on the figures, the cup was deemed to be seated at the end of rebound 1 because of excessive plastic deformation and bone fracture during the second impact.

Convergence was achieved in the third analysis; the change in total internal energy was within two percent, as shown in Table 13.

Table 13: Total Internal Energies of the 3D Model Analyses
Total internal energy at the end of rebound 1 for each analysis in the anatomically accurate model. The greatest absolute difference in total internal energy relative to the third analysis is shown.

Analysis No.	Total Internal Energy (J)	% $\|\Delta\|_{Max}$
1	4.466	–
2	4.351	–
3	4.434	1.9

Plots of radial cup deformation, as measured by a spherical coordinate system located at the centre of the cup in the original cup rim plane, were generated from analysis 3 at the height of impact and at the end of cup rebound. These plots are shown in Figure 31.

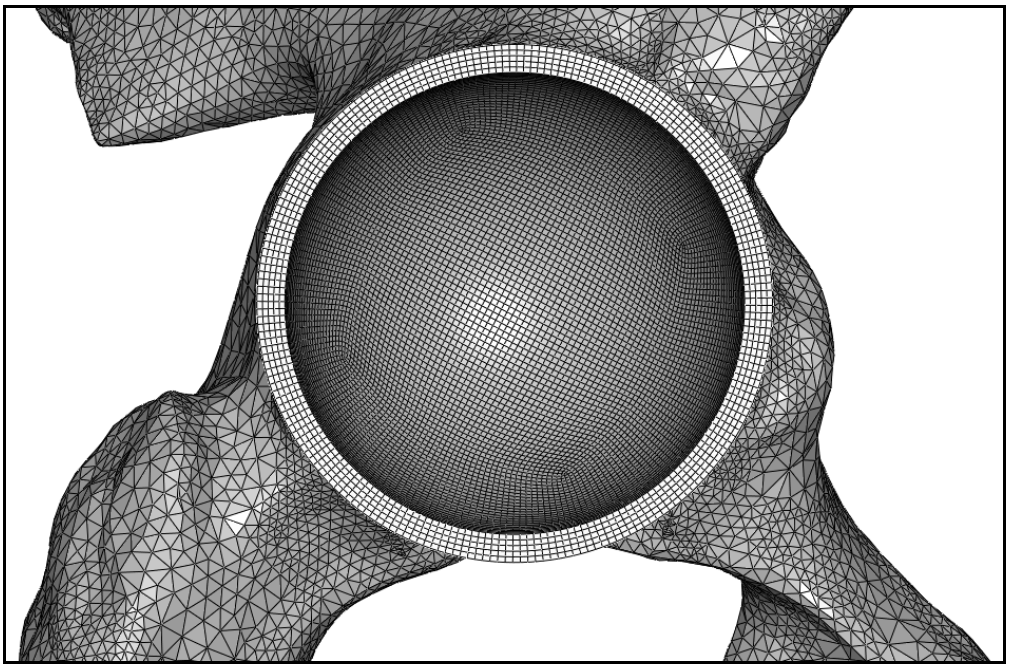

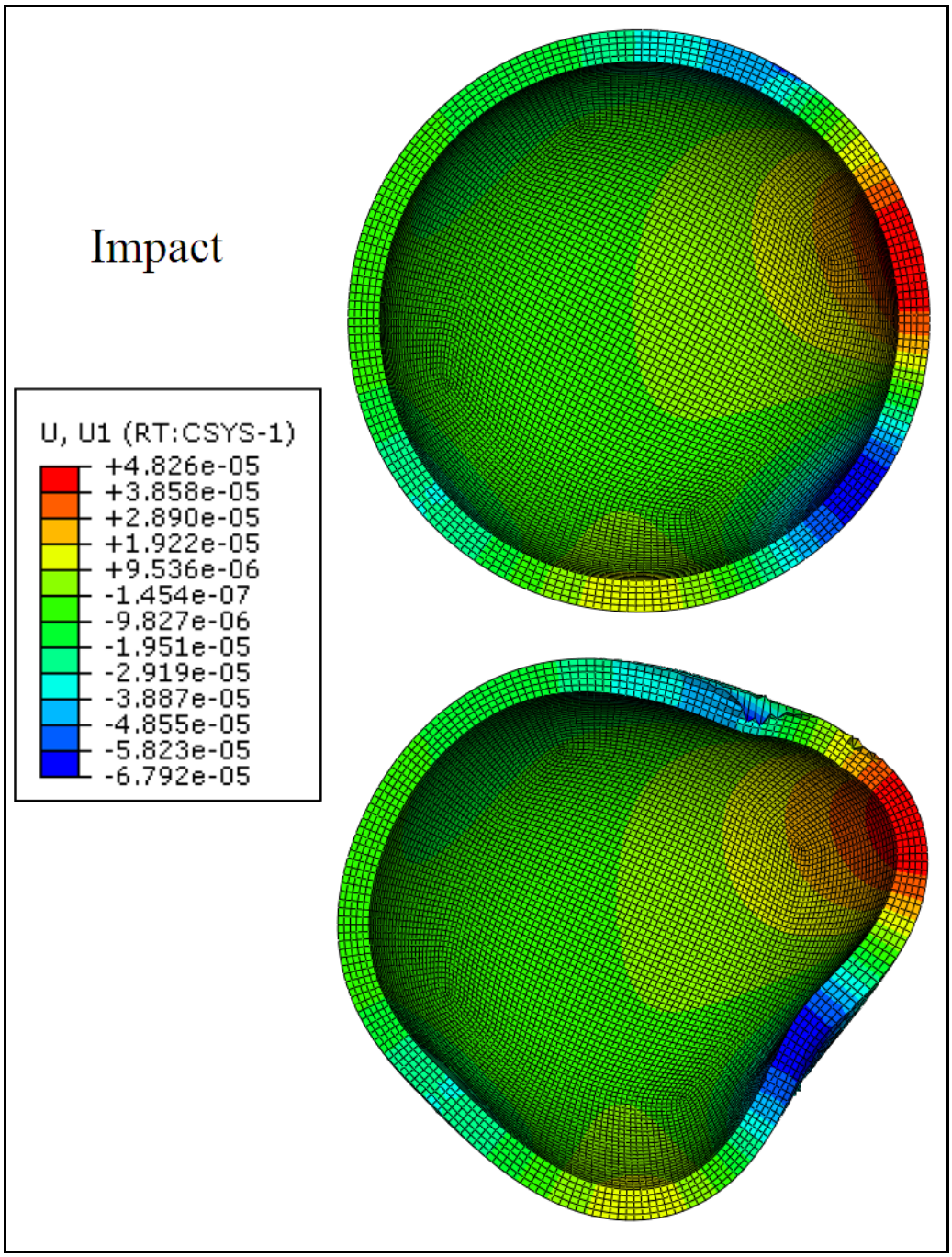
Impact
U, U1 (RT:CSYS-1)
+4.826e-05
+3.858e-05
+2.890e-05
+1.922e-05
+9.536e-06
-1.454e-07
-9.827e-06
-1.951e-05
-2.919e-05
-3.887e-05
-4.855e-05
-5.823e-05
-6.792e-05

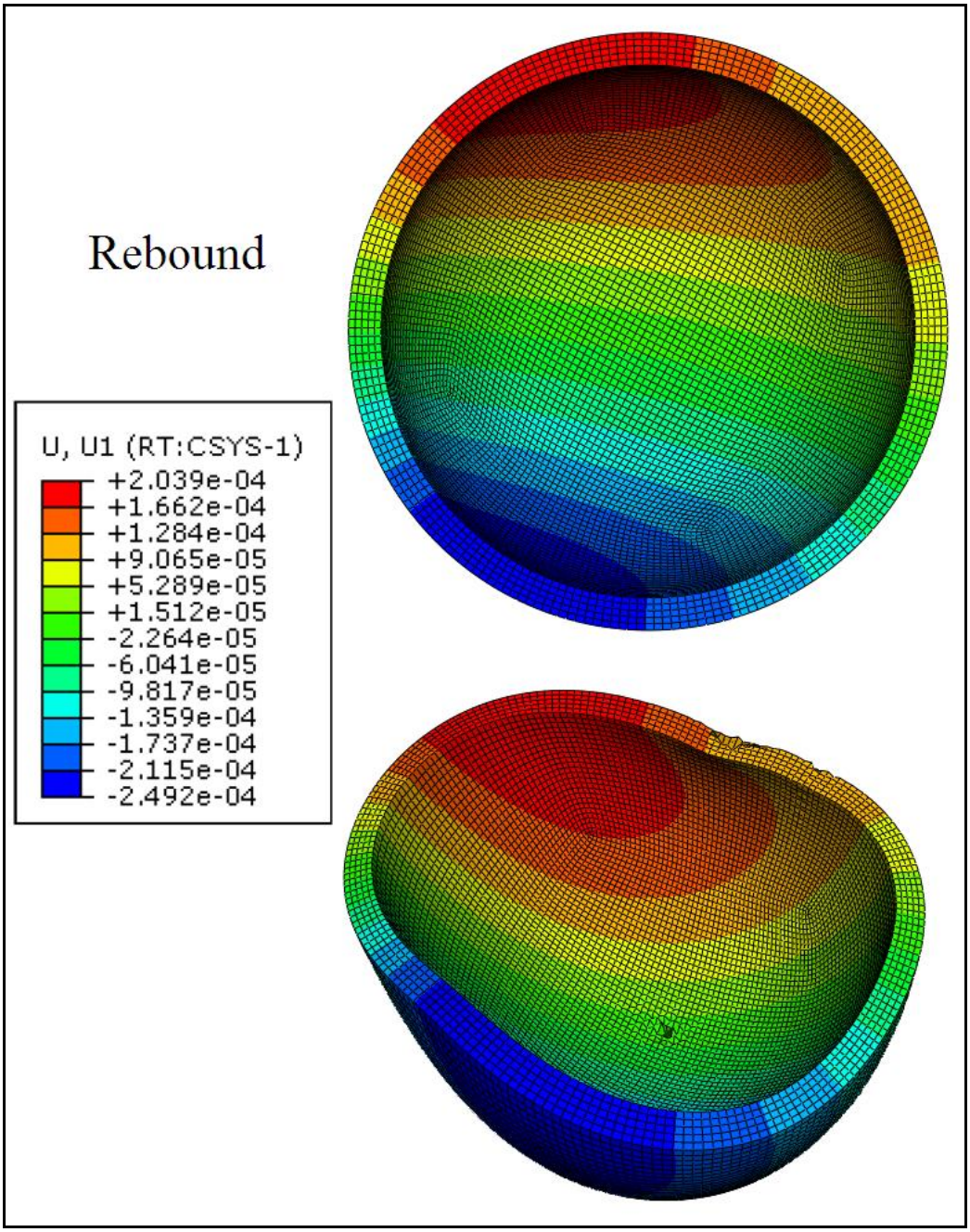

Figure 31: 3D Model Radial Cup Deformation
Contour plots of radial cup deformation after impact and rebound, as determined via a spherical coordinate system located at the centre of the cup in the original cup rim plane. The first panel shows the reference position of the cup. In each set of cup deformation contour plots, the first plot is unscaled, and the second is scaled 100 times. (+) indicates expansion and (-) indicates compression, relative to the original cup shape. Units in metres.

During impact of the cup into the acetabulum, the cup radial deformation ranged from -68 to +48 μm. The cup walls were compressed between the superior-anterior rim at the ilium, the inferior-anterior rim at the pubis, and slightly at the inferior-posterior rim at the ischium. At the end of rebound, the cup was compressed (i.e., 'pinched') predominantly between the ischial and ilial columns – similar to what was observed by Jin et al. (2006) in their cadaver experiments – with deformations ranging from -249 to +204 μm. The deformations during impact appear to be in agreement with previously reported cup deformation results; Udofia et al. (2007) reported radial rim deformations as high 49 μm in their 1 mm press-fit 3D anatomically accurate finite element model. The deformations during rebound, however, are much higher and therefore appear to be improbable. The discrepancy between the impact and rebound deformations may be attributed to incompatibility of the spherical coordinate system with the severe out-of-plane rim warping of the cup during rebound, shown in Figure 32. Releasing the constraints on the cup after rebound had little effect on the deformed shape of the cup. This is not surprising, as the cup only rotated 0.36° after the constraints were removed.

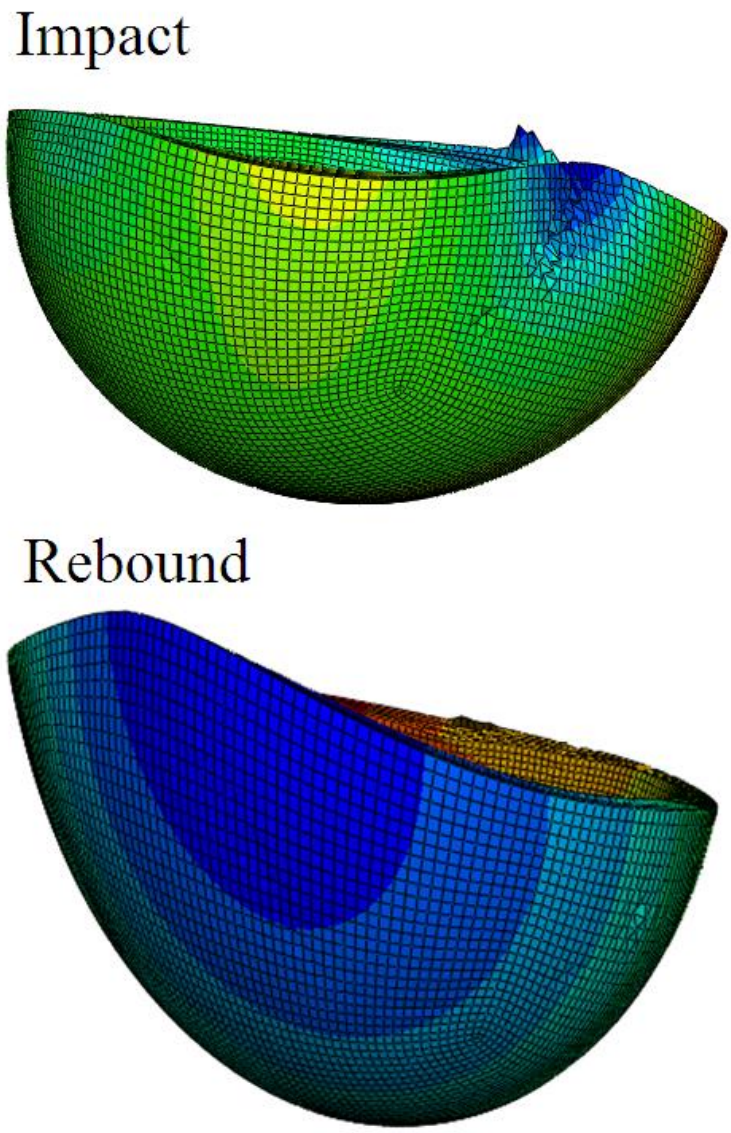

Figure 32: Cup Rim Warping
Scaled (100X) side profiles of the cup at the height of impact and at the end of rebound showing out-of-plane warping of the cup rim.

The irregular deformation (i.e., pinching and rim warping) of the cup is in sharp contrast to the symmetrical cup deformation in the simple 3D model of Yew et al. (2006), wherein diametral deformation measurements at the rim were used to characterize cup deforma-

tion. The irregular shape of the cup in this thesis renders diametral deformation measurements at the cup rim meaningless because bearing clearance is likely to be compromised elsewhere. Thus, a full characterization of cup deformation in 3D is necessary.

During press-fitting, plastic deformation of the cup may be possible. Unfortunately, previous resurfacing cup deformation studies did not specify CoCr yield behaviour, and so plastic deformation could not be modeled. In this thesis, a small amount of plastic deformation occurred in the cup near the superior-anterior rim at the ilium at the height of impact, as shown in Figure 33. This is especially relevant after the bone surrounding the cup relaxes over time, as the cup may not return to its original undeformed shape.

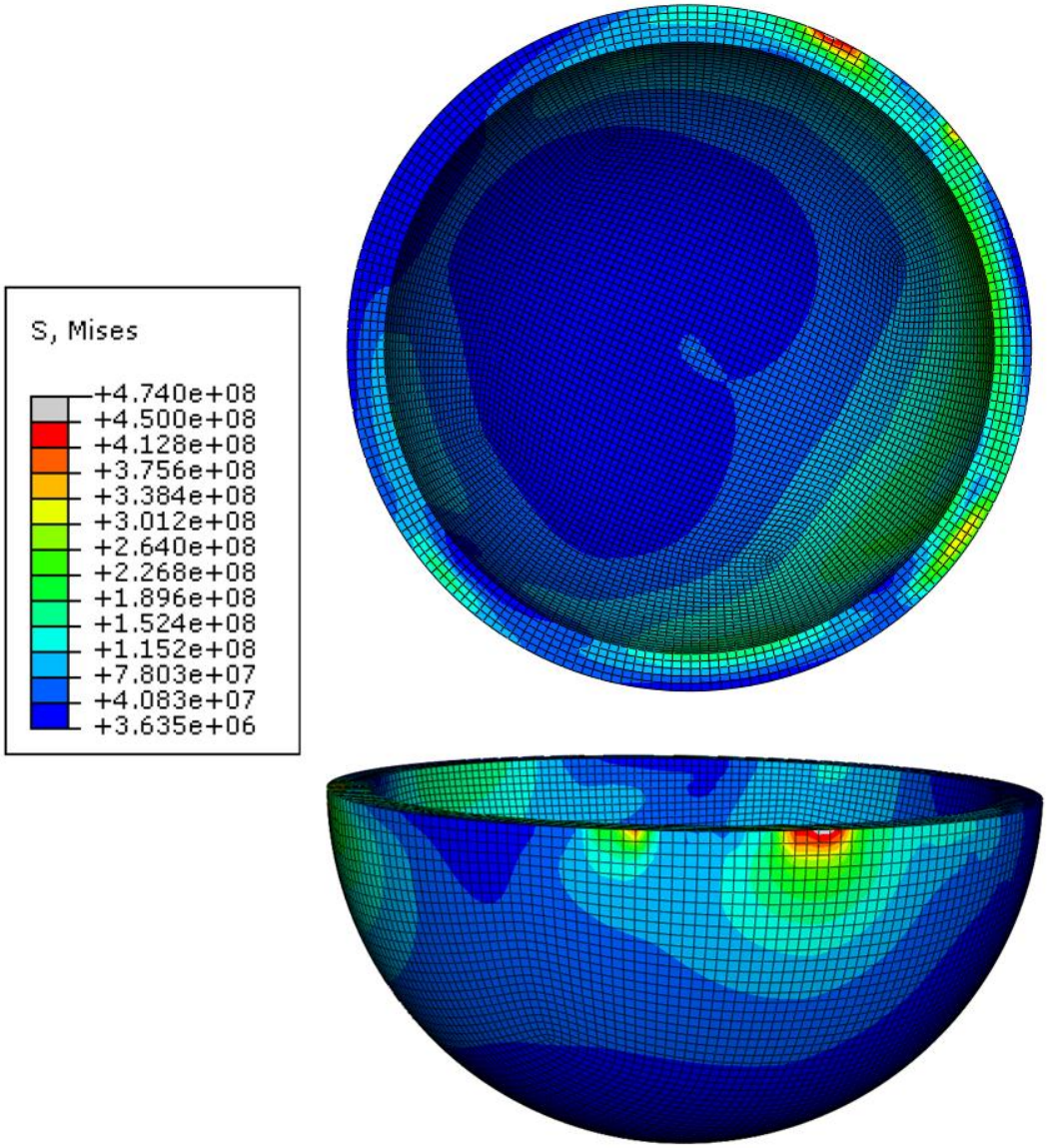

Figure 33: Cup Von Mises Stresses
Von Mises stresses in the cup at the height of impact. Stress reaching or exceeding the yield stress of CoCr is shown in red (and grey) to represent plastic deformation of the cup. Plastic deformation occurred in the cup rim near the superior-anterior rim at the ilium. Units in pascals.

Chapter 5

Conclusions and Recommendations

In this thesis, a three-dimensional finite element model of resurfacing cup deformation that addressed the limitations of previous models in terms of pelvic geometry, meshing, cup and bone material properties, and cup insertion, was created. Measurement of diametral deformation at the rim of the resurfacing cup for characterization of cup deformation is shown in this thesis to be insufficient; full characterization of cup deformation in three-dimensions is necessary.

Several modeling limitations that could potentially have a significant impact on cup deformation remain. Regarding the geometries used in the 3D model of this thesis, deficiencies are present in the hemi-pelvis, cup, and impactor. In the hemi-pelvis geometry, reaming of the acetabulum was simulated by subtracting a sphere from the acetabulum, thus producing a perfectly spherical cavity. In reality, however, a reamed acetabulum has non-uniform geometry, which could have a pronounced effect on cup deformation. As such, reaming should not be simulated, but rather reaming should be performed by a surgeon before the model geometry is created. In the cup geometry, solid CoCr was assumed in lieu of the 1 mm thick beaded exterior. Unfortunately, this could affect cup de-

formation via differences in cup stiffness and contact properties. Future studies could investigate how the beaded exterior can be modeled more realistically. The impactor geometry was also simplified, but more so than the hemi-pelvis and cup geometries. An impactor consists of a long handle attached to the cup rim via wires tensioned through a polyethylene insert; this was represented by a rigid plate geometry in this thesis. This simplification could be the reason why severe cup rim warping was observed in the model. Modeling a more realistic impactor could potentially eliminate excessive rim warping, in which case a spherical coordinate system may successfully be used to measure cup deformation at the end of cup rebound. In addition, realistic constraints could be applied to the impactor handle instead of constraining the cup pole to simulate the stabilizing forces applied by the surgeon during press-fitting for prevention of cup rotation. This could have a significant impact on the stress distributions (and therefore deformation) around the rim of the cup.

Laser scanning of a hemi-pelvis replica was used in this thesis to obtain the 3D hemi-pelvis geometry because Computed Tomography (CT) of an actual hemi-pelvis (cadaver or in vivo) was not possible within the budgetary constraints. Computed Tomography is ideal because it allows for the acquisition of a wider array subject-specific geometries that also include heterogeneous bone material properties (via density-modulus relationships), and it requires less effort (Ong et al. 2006). In this thesis, difficulties were encountered with geometry creation using laser-scanned data. Specifically, creation of a separate cortical layer via a cortical/cancellous boundary geometry in order to assign separate cortical and cancellous bone properties in the 3D model proved to be difficult and time consuming. Also, initial attempts at simulated reaming of the geometry gener-

ated thin regions of cortical bone that presented meshing difficulties. As such, a reaming configuration that resulted in a larger cavity than initially planned had to be used in order to avoid generating the thin regions; this may have resulted in the use of an oversized cup geometry.

Material properties is another aspect in which the models of this thesis are limited. Although the specification of yield behaviour is a significant advancement over previous finite element models, the bone properties were still very simplistic in that homogeneity and isotropy were assumed, and viscoelasticity was not considered. Such simplifications could have a pronounced effect on overall cup deformation. An example is that cup deformation may have been underestimated due to the lack of viscoelastic response of increased bone stiffness during impact (Spears et al. 1999). Therefore, to obtain more realistic finite element models, future modeling efforts should include heterogeneous and anisotropic bone material properties, as well as viscoelasticity.

Limitations were also present in the aspects of cup positioning and press-fitting for simulation of cup insertion. Regarding positioning of the cup within the acetabulum prior to press-fitting simulation, clinical inclination and anteversion could only be estimated (via a plane fit to the acetabular rim), as an appropriate frame of reference was unavailable. In future work, a frame of reference can be established for a hemi-pelvis geometry if the full pelvis or matching femur geometry is available (Udofia et al. 2007). For press-fitting simulation, this thesis determined that the multiple-displacement method was the best of the available methods for use in the 3D model. This method may not be appropriate because it is static-based (i.e., time-invariant), and press-fitting is a dynamic process. The fact that only one impact was required to seat the cup in this thesis exemplifies this.

Also, previous FEA studies showed that cup seating could only be achieved with increasing magnitude impacts, in contrast to clinically-representative constant magnitude impacts (Spears et al. 1999). More realistic press-fitting simulation may be achieved with a dynamic method that includes impactor momentum and impact duration considerations. Finally, another limitation is that simplistic constraints were applied to the pelvis during press-fitting. Whether or not more realistic muscular and ligamentous forces acting on the pelvis has an effect on cup deformation remains to be established.

To further improve upon finite element modeling of resurfacing cup deformation, future work should involve clinical experimentation, validation, and development of additional methods of characterizing cup deformation. Clinical experimentation is necessary to obtain more realistic loads and constraints during press-fitting. For example, impact forces could be measured experimentally and used as model inputs. Experimental validation is necessary to firmly establish model credibility; it would consist of implanting resurfacing cups into cadaver or replica hemi-pelvises, followed by cup deformation measurement via a coordinate measurement machine (Yew et al. 2006). For characterizing cup deformation, a suggested alternative is to find the ‘centre’ of the deformed cup by computing the mean over the spatial coordinates of the points defining the cup interior. The minimum distance between the centre point and the cup interior could then be obtained and compared to the radius of the matching femoral head.

References

Adams, V. and A. Askenazi. 1999. *Building Better Products with Finite Element Analysis*. Sante Fe: OnWord Press.

Amirouche, F., M. Gonzalez and L. Aram. 2006. Hip biomechanics. *Encyclopedia of Biomaterials and Biomedical Engineering*, ed. G.L. Bowlin and G. Wnek, 1-17. London: Taylor & Francis Group.

Anderson, A.E., B.J. Ellis and J.A. Weiss. 2007. Verification, validation and sensitivity studies in computational biomechanics. *Computer Methods in Biomechanics and Biomedical Engineering* 10(3): 171-184.

Anderson, A.E., C.L. Peters, B.D. Tuttle and J.A. Weiss. 2005. Subject-specific finite element model of the pelvis: development, validation and sensitivity studies. *Journal of Biomechanical Engineering* 127: 364-373.

Beaupré, G.S. and D.R. Carter. 1992. Finite element analysis in biomechanics. *Biomechanics: Structures and Systems*, ed. A.A. Biewener, 149-174. Oxford: Oxford University Press.

Beevers, A., S.M. Steidler, J. Durodola and M. Coackley. 2001. Analysis of stiffness of adhesive joints in car bodies. *Journal of Materials Processing Technology* 118: 96-101.

Bellini, C.M., F. Galbusera, R.G. Ceroni and M.T. Raimondi. 2007. Loss in mechanical contact of cementless acetabular prostheses due to post-operative weight bearing: a biomechanical model. *Medical Engineering & Physics* 29: 175-181.

Buckwalter, J.A. and G. Etienne. 2006. Osteoarthritis and inflammatory arthritis. *Orthopaedic Knowledge Update: Hip and Knee Reconstruction 3*, ed. R.L. Barrack, R.E. Booth, Jr., J.H. Lonner, J.C. McCarthy, M.A. Mont and H.E. Rubash, 187-198. American Academy of Orthopaedic Surgeons.

Burnell, C. (2007). Discussion with Dr. Colin Burnell, Orthopaedic Surgeon with the Concordia Joint Replacement Group (CJRG), Winnipeg, MB, Canada. August 2, 2007. N. Kesler.

Cezayirlioglu, H., E. Bahniuk, D.T. Davy and K.G. Heiple. 1985. Anisotropic yield behavior of bone under combined axial force and torque. *Journal of Biomechanics* 18(1): 61-69.

CIHI (2009). Canadian Joint Replacement Registry (CJRR) 2008-2009 Annual Report - Hip and Knee Replacements in Canada. Ottawa, Canadian Institute for Health Information.

Dalstra, M., R. Huiskes and L.v. Erning. 1995. Development and validation of a three-dimensional finite element model of the pelvic bone. *Journal of Biomechanical Engineering* 117: 272-278.

Dalstra, M., R. Huiskes, A. Odgaard and L.v. Erning. 1993. Mechanical and textural properties of pelvic trabecular bone. *Journal of Biomechanics* 26(4/5): 523-535.

Desai, C.S. and J.F. Abel. 1972. *Introduction to the Finite Element Method: A Numerical Method for Engineering Analysis*: Litton Educational Publishing, Inc.

Doblaré, M., J.M. García and M.J. Gómez. 2004. Modelling bone tissue fracture and healing: A review. *Engineering Fracture Mechanics* 71: 1809-1840.

Ebied, A. and S. Journeaux. 2003. Metal-on-metal hip resurfacing. *Current Orthopaedics* 16: 420-425.

Gilbert, J.L. 2007. Metals. *The Adult Hip*, ed. J.J. Callaghan, A.G. Rosenberg and H.E. Rubash, 128-143. Philadelphia: Lippincott Williams & Wilkins.

Huo, M.H., J. Parvizi, B.S. Bal and M.A. Mont. 2008. What's new in total hip arthroplasty. *The Journal of Bone and Joint Surgery* 90(A): 2043-2055.

Jin, Z.M., S. Meakins, M.M. Morlock, P. Parsons, C. Hardaker, M. Flett and G. Isaac. 2006. Deformation of press-fitted metallic resurfacing cups. Part 1: experimental simulation. *Proceedings of the Institution of Mechanical Engineers - Part H: Journal of Engineering in Medicine* 220: 299-309.

Katz, J.L., C.G. Ambrose, C. McMillin and P. Spencer. 2004. Orthopedic biomaterials. *Encyclopedia of Biomaterials and Biomedical Engineering*, ed. G.L. Bowlin and G. Wnek, 1160-1171. New York: Marcel Dekker, Inc.

Kopperdahl, D.L. and T.M. Keaveny. 1998. Yield strain behavior of trabecular bone. *Journal of Biomechanics* 31: 601-608.

Langton, D.J., S.S. Jameson, T.J. Joyce, J. Webb and A.V.F. Nargol. 2008. The effect of component size and orientation on the concentrations of metal ions after resurfacing arthroplasty of the hip. *The Journal of Bone and Joint Surgery* 90(B)(9): 1143-1151.

Logan, D.L. 2002. *A First Course in the Finite Element Method*, 3rd ed. Pacific Grove, CA: Wadsworth Group.

Luo, Y. and U. Häussler-Combe. 2003. A gradient-based adaptation procedure and its implementation in the element-free Galerkin method. *International Journal for Numerical Methods in Engineering* 56: 1335-1354.

Marks, L.W. and T.N. Gardner. 1993. The use of strain energy as a convergence criterion in the finite element modelling of bone and the effect of model geometry on stress convergence. *Journal of Biomedical Engineering* 15: 474-476.

Ong, K.L., S.M. Kurtz, M.T. Manley, N. Rushton, N.A. Mohammed and R.E. Field. 2006. Biomechanics of the Birmingham hip resurfacing arthroplasty. *The Journal of Bone and Joint Surgery* 88-B(8): 1110-1115.

Ong, K.L., M.T. Manley and S.M. Kurtz. 2008. Have contemporary hip resurfacing designs reached maturity? A review. *The Journal of Bone and Joint Surgery* 90(A): 81-88.

Phillips, A.T.M., P. Pankaj, C.R. Howie, A.S. Usmani and A.H.R.W. Simpson. 2007. Finite element modelling of the pelvis: inclusion of muscular and ligamentous boundary conditions. *Medical Engineering & Physics* 29: 739-748.

Phillips, A.T.M., P. Pankaj, C.R. Howie, A.S. Usmani and A.H.R.W. Simpson. 2006. 3D non-linear analysis of the acetabular construct following impaction grafting. *Computer Methods in Biomechanics and Biomedical Engineering* 9(3): 125-133.

Ramos, A. and J.A. Simões. 2006. Tetrahedral versus hexahedral finite elements in numerical modelling of the proximal femur. *Medical Engineering and Physics* 28: 916-924.

Roberts, P., P. Grigoris, H. Bosch and N. Talwaker. 2005. Resurfacing arthroplasty of the hip. *Current Orthopaedics* 19: 263-279.

Schmalzried, T.P. and W.H. Harris. 1992. The Harris-Galante porous-coated acetabular component with screw fixation. *The Journal of Bone and Joint Surgery* 74-A(8): 1130-1139.

Shim, K.W., D.J. Monaghan and C.G. Armstrong. 2002. Mixed dimensional coupling in finite element stress analysis. *Engineering with Computers* 18: 241-252.

Shimmin, A., P.E. Beaulé and P. Campbell. 2008. Metal-on-metal hip resurfacing athroplasty. *The Journal of Bone and Joint Surgery* 90(A): 637-654.

Shirazi-Adl, A., M. Dammak and G. Paiement. 1993. Experimental determination of friction characteristics at the trabecular bone/porous-coated metal interface in cementless implants. *Journal of Biomedical Materials Research* 27: 167-175.

Simulia. 2007. *ABAQUS Version 6.7 Documentation*: Dassault Systèmes, Lowell, MA.

Spears, I.R., M.M. Morlock, M. Pfleiderer, E. Schneider and E. Hille. 1999. The influence of friction and interference on the seating of a hemispherical press-fit cup: a finite element investigation. *Journal of Biomechanics* 32: 1183-1189.

Spears, I.R., M. Pfleiderer, E. Schneider, E. Hille, G. Bergmann and M.M. Morlock. 2000. Interfacial conditions between a press-fit acetabular cup and bone during daily activities: implications for achieving bone in-growth. *Journal of Biomechanics* 33: 1471-1477.

Spears, I.R., M. Pfleiderer, E. Schneider, E. Hille and M.M. Morlock. 2001. The effect of interfacial parameters on cup-bone relative micromotions: a finite element investigation. *Journal of Biomechanics* 34: 113-120.

Stolk, J., N. Verdonschot and R. Huiskes. 2001. Management of stress fields around singular points in a finite element analysis. *Computer Methods in Biomechanics and Biomedical Engineering*, ed. J. Middleton, M.L. Jones, N.G. Shrive and G.N. Pande, 57-62. London: Gordon and Breach Science Publishers.

Turgeon, T.R. (2009). Discussion with Dr. Thomas R. Turgeon, Orthopaedic Surgeon with the Concordia Joint Replacement Group (CJRG), Winnipeg, MB, Canada. April 5, 2009. N. Kesler.

Udofia, I., F. Liu, Z. Jin, P. Roberts and P. Grigoris. 2007. The initial stability and contact mechanics of a press-fit resurfacing arthroplasty of the hip. *The Journal of Bone and Joint Surgery* 89-B(4): 549-556.

Widmer, K.-H., B. Zurfluh and E.W. Morscher. 2002. Load transfer and fixation mode of press-fit acetabular sockets. *The Journal of Arthroplasty* 17(7): 926-935.

Yew, A., Z.M. Jin, A. Donn, M.M. Morlock and G. Isaac. 2006. Deformation of press-fitted metallic resurfacing cups. Part 2: finite element simulation. *Proceedings of the Institution of Mechanical Engineers - Part H: Journal of Engineering in Medicine* 220: 311-319.

Zienkiewicz, O.C., R.L. Taylor and J.Z. Zhu. 2005. *The Finite Element Method: Its Basis and Fundamentals*, 6th ed. Burlington, MA: Elsevier Butterworth-Heinemann.